OFFICE OF CIVILIAN RADIOACTIVE WASTE MANAGEMENT
ANALYSIS/MODEL COVER SHEET

1. QA: QA

Page: 1 of: 64

Complete Only Applicable Items

2. ☒ Analysis — Check all that apply

Type of Analysis	☐ Engineering ☐ Performance Assessment ☒ Scientific
Intended Use of Analysis	☐ Input to Calculation ☒ Input to another Analysis or Model ☒ Input to Technical Document ☐ Input to other Technical Products

Describe use:

Predictions of cladding degradation

3. ☒ Model — Check all that apply

Type of Model	☐ Conceptual Model ☐ Abstraction Model ☒ Mathematical Model ☐ System Model ☐ Process Model
Intended Use of Model	☐ Input to Calculation ☒ Input to another Model or Analysis ☐ Input to Technical Document ☐ Input to other Technical Products

Describe use:

Model for cladding degradation

4. Title:

Clad Degradation - Dry Unzipping

5. Document Identifier (including Rev. No. and Change No., if applicable):

ANL-EBS-MD-000013 REV 00

6. Total Attachments:

N/A

7. Attachment Numbers - No. of Pages in Each:

N/A

	Printed Name	Signature	Date
8. Originator	Brady Hanson	Christine Stockman for Brady Hanson	4/21/00
9. Checker	David Stahl	Raymond Wu for DS	4/21/00
10. Lead/Supervisor	Christine Stockman	Christine Stockman	4/21/00
11. Responsible Manager	David Stahl	Raymond Wu for DS	4/21/00

12. Remarks:

OFFICE OF CIVILIAN RADIOACTIVE WASTE MANAGEMENT
ANALYSIS/MODEL REVISION RECORD

Complete Only Applicable Items

2. Analysis or Model Title:

Clad Degradation - Dry Unzipping

3. Document Identifier (including Rev. No. and Change No., if applicable):

ANL-EBS-MD-000013 REV 00

4. Revision/Change No.	5. Description of Revision/Change
00	Initial Issue

CONTENTS

Page

CONTENTS (Continued)

Page

FIGURES

Page

TABLES

Page

ACRONYMS AND ABBREVIATIONS

BWR	boiling water reactor
CANDU	Canada Deuterium
CSNF	commercial spent nuclear fuel
LRB	laboratory record book
LWR	light water reactor
O/M	oxygen-to-metal ratio
PNNL	Pacific Northwest National Laboratory
PWR	pressurized water reactor
SEM	scanning electron microscope
TGA	thermogravimetric analysis
XRD	x-ray diffraction

1. PURPOSE

The purpose of this analysis is to provide a current summary of data and develop a semi-empirical model for cladding degradation, i.e., unzipping, due to dry-air oxidation of commercial light water reactor (LWR) spent nuclear fuel (CSNF). Spent fuel oxidation is a concern to repository design for two reasons. First, as the fuel oxidizes to U_3O_8 or higher oxidation states, as is thermodynamically predicted, the smaller density of these higher oxides results in a volume expansion of greater than 36%. The fuel can thus stress the cladding, further opening existing defects and increasing the surface area of fuel that potentially may be exposed directly to groundwater. Second, U_3O_8 has a higher specific dissolution rate than UO_2, which, when combined with the larger surface area created by spallation of the less dense phase, results in a dissolution rate a factor of about 150 higher than that of the UO_2 (Gray and Wilson 1995, p. 4.12). Even formation of the intermediate phase U_4O_{9+x}, which exhibits dissolution behavior similar to UO_2 and is slightly more dense, may increase the exposed surface area of fuel due to the opening of grain boundaries and cracking of the grains resulting from the stresses imposed by the volume contraction as the $UO_{2.4}$ phase forms.

The analysis and model presented here is semi-empirical in nature. Other than a simple model to determine the extent of reaction for a given bulk oxidation state, the analysis uses simple linear regression fits to data obtained at Pacific Northwest National Laboratory (PNNL) from oxidation tests on bare CSNF fragments. The oxidation data used for this analysis was obtained from thermogravimetric analysis (TGA) testing over the temperature range 255°C to 325°C and used a dry- air atmosphere. The fuels tested had burnups in the range 16 MWd/kg M to about 70 MWd/kg M, but only the data up to a burnup of about 42 MWd/kg M were used for the model development. Results obtained, using the model for parameters outside of these ranges, are based on extrapolation of the model. However, the model results are compared to literature data to provide an independent verification of the model over the largest possible range. This model is also limited in that there is no explicit dependence on the grain size of the fuel; what dependence that exists appears only in the oxygen-to-metal (O/M) ratio as a function of time data. The results obtained are valid for a nominal analysis, but it must be stressed that smaller-grained fuels would be expected to oxidize more rapidly and, conversely, fuels with larger-grains would take longer to oxidize. However, the present semi-empirical model does not allow such effects to be quantified. The effect of moisture on the rate of oxidation specifically on the rate of U_3O_8 formation is unclear because of conflicting information reported in literature.

The primary results obtained from this model are the time required for oxidation of CSNF from UO_2 to $UO_{2.4}$, the time required for an existing cladding flaw to begin to propagate due to subsequent U_3O_8 formation (i.e., incubation time), and the velocity at which a crack propagates and "unzips" the cladding. The oxidation results, including the estimated incubation times, are dependent on the burnup and temperature of the fuel and cladding unzipping velocities are also dependent on the cladding's mechanical properties. Where necessary, conservative assumptions are made such that the times predicted by the model would be faster than those that may occur under repository conditions.

This report was developed in accordance with the Development Plan for *Waste Package Materials Department Analysis and Modeling Reports Supporting the Waste Form PMR*

(CRWMS M&O 2000). It specifically addresses the item, "Clad Degradation–Dry Unzipping" of the product development plan and is in compliance with procedure AP-3.10Q.

2. QUALITY ASSURANCE

The Quality Assurance (QA) program applies to this analysis. All types of waste packages were classified (per QAP-2-3) as Quality Level-1. This analysis applies to all of the waste package designs included in the MGR Classification Analyses. Reference CRWMS M&O (1999a) *Classification of the MGR Uncanistered Spent Nuclear Fuel Disposal Container System* is cited as an example. The development of this analysis is conducted under activity evaluation *1101213FM3 Waste Form Analyses & Models - PMR* (CRWMS M&O 1999b) which was prepared per QAP-2-0. The results of that evaluation were that the activity is subject to the *Quality Assurance Requirements and Description* (DOE 2000) requirements.

3. COMPUTER SOFTWARE AND MODEL USAGE

No standard commercial or user developed software applications were used in preparing this AMR.

4. INPUTS

4.1 DATA AND PARAMETERS

The only oxidation data used directly to derive the parameters (see Sections 6.3.2, 6.4.1 and 6.4.2) for the model were obtained at PNNL by TGA testing of bare commercial spent nuclear fuel (CSNF) fragments. These data are found in Table 1 and Table 2 in Section 6.1.1. Documentation of the fits to the data to obtain the model parameters was developed in PNNL (1999), Laboratory Record Book (LRB) 57225 (DTN: LL000402951021.133). All TGA data have been documented (DTN: LL000314651021.132) and submitted to the Project. Oxidation data from oven dry-bath tests conducted at 175°C, 195°C, and 255°C were used to validate the extrapolation of the model parameters to these temperatures (see Section 6.3.2). These dry-bath data have also been documented (Hanson 1998). The fuels tested were taken from fuel rods that had been extensively characterized (see Table 4, Section 6.1.3) by the Materials Characterization Center at PNNL (Guenther 1988a, Guenther 1988b, Guenther 1991a, Guenther 1991b). The characteristics of the fuel phases formed during dry-air oxidation (see Table 3, Section 6.1.2) are taken from various literature sources and documented in Hanson (1998). The thermo-mechanical properties of Zircaloy necessary for calculating the cladding unzipping velocity (see Section 6.6) are assumed to be those of unirradiated Zircaloy (see Table 5, Section 6.1.4), as presented by Glasstone and Sesonske (1994, Table A.6, p. 486). A literature review (see Table 6, Section 6.1.6) of incubation times and cladding unzipping velocities is presented for comparison and validation of the model (See Table 17 and Table 19). Finally, a literature review (see Section 6.1.5) of the possible effects of moisture on oxidation of CSNF is given.

Data used in this AMR are not directly used in producing a technical product that provides any estimates for any of the principal factors or potentially disruptive events and processes and is thus labeled qualified verification level 2.

4.2 CRITERIA

No criteria apply to this analysis or model.

4.3 CODES AND STANDARDS

The methodology used in the data collection and model development conforms with the practice of Accelerated Tests, as outlined in the American Society for Testing and Materials (ASTM) "Standard Practice for Prediction of the Long-Term Behavior of Waste Package Materials Including Waste Forms in the Geologic Disposal of High-Level Nuclear Waste" (C1174-97). No other codes or standards have been used in the derivation of the model.

5. ASSUMPTIONS

- The O/M ratio of spent fuel is assumed to be 2.00 prior to emplacement in the repository. This assumption is based on the experimental work described in Hanson (1998, Section 2.4.3). Oxidation during reactor operations and pool storage should be minimal (Section 6.1.5.2). At least one rod that failed during reactor operation was examined by Kohli et al. (1985, p. 192) and was identified as having a starting O/M of 2.33. However, it is not known when the oxidation occurred or how extensive it was. Fuels with higher starting O/M ratios would have shorter incubation times (Section 6.5), but only fuel that failed prior to emplacement would possibly be affected.

- Based on the experimental work described in Hanson (1998, Section 2.2.2), the oxidation of CSNF is assumed to proceed via a two-step reaction where no $UO_{2.75}$ (U_3O_8) is formed until conversion of a grain to $UO_{2.4}$ (U_4O_9) is complete. This may not be true for fuels of lower burnup (<20 MWd/kg M). The incubation times (Section 6.5) would be greatly reduced for these fuels. However, the bounding case fits were on low-burnup samples that may have had both oxidation transitions occurring simultaneously. At worst, the bounding case parameters could be used for performance assessment.

- The difference in molecular weight due to the variable ^{235}U content and the replacement of uranium ions with fission products and higher actinides are ignored. This was done in calculating the Δ(O/M) from the TGA data. If there is an impact, it would affect all data and simply shift the actual O/M over the entire oxidation history of a sample, and is, therefore, not significant. Further, it is assumed that the molecular weight of uranium is 238 g mol^{-1} and of oxygen is 16 g mol^{-1}, introducing only negligible uncertainty (Table 3, Section 6.1.2).

- The densities of the $UO_{2.4}$ and $UO_{2.75}$ phases formed (Section 6.1.2) are assumed identical to the stoichiometric phases U_4O_9 and U_3O_8, respectively. This is probably conservative since the hyperstoichiometric phases have a higher mass due to oxygen uptake in interstitial sites, with minimal impact on the lattice parameter. The densities affect the parameters z_1 and z_2 in Section 6.

- The burnup dependence (Section 6.4.1) of the activation energy is assumed to be linear (Hanson 1998, Equation 5.2, p. 5.16; McEachern et al. 1998, Equation 9 p. 147). The actual dependence of the oxidation is on total soluble impurity content (Hanson 1998, Section 5.2.5), but for this analysis, this value is well approximated by burnup.

- It is assumed that the burnup dependence of the $UO_{2.4} \rightarrow UO_{2.75}$ transition is valid for low burnups (<16 MWd/kgM) and high burnups (>42 MWd/kgM), beyond the scope of the data used in this analysis. This assumption was used to calculate incubation times (Section 6.5) and unzipping velocities (Section 6.6) over the range of burnups 0 to 50 MWd/kgM. Further, it is assumed that there is no change in mechanisms or activation energies for either transition at temperatures below those tested (175°C dry-bath data) as part of this program. There is no evidence that such changes have been observed or suspected for the temperature range of interest to the repository (i.e., <350°C).

- Oxidation of the fuel is assumed to be isotropic (Sections 6.5 and 6.6). While this may not be a conservative assumption, it appears realistic given the comparison with literature unzipping values.

- Based on the review of literature (Section 6.1.5), it is assumed that the presence of moisture during oxidation will increase the rate of oxidation, but that the incubation times (Section 6.5) and unzipping velocities (Section 6.6) will be within the range predicted by the bounding case of this model. Confirmatory testing is underway to validate this assumption.

- The thermo-mechanical properties (G, E, ν, σ_{yield}) of irradiated Zircaloy are assumed to be identical to those of unirradiated Zircaloy (Section 6.1.4). The unzipping velocities (Section 6.6 and 6.6.1) are conservative by a factor of 2 to 3. This conservatism is a result of the much smaller yield strength for unirradiated Zircaloy (CRWMS M&O 1998).

- The fuel/clad gap upon emplacement is assumed to be zero. This is the most conservative assumption that can be made with respect to the incubation time calculations (Section 6.5).

- It is assumed that zero strain is needed to initiate crack growth at an existing defect. This is the most conservative assumption that can be made with respect to the incubation time calculations (Section 6.5).

- It is assumed that all grains have equal access to an unlimited oxygen supply. No consideration for oxygen depletion or transport limitations was made. There is also no grain boundary transport/oxidation necessary before all grains oxidize. These assumptions are inherently conservative, promoting more rapid oxidation than would be expected (Section 6).

- The fuel in the local region of the defect or crack opening is approximated as a single spherical grain (Sections 6.3.1, 6.4.3, 6.5, and 6.6). The equations derived are identical for cubic grains or cylindrical grains with radius and height r. This assumption is equivalent to a multi-grain sample of equivalent grains with an ideal packing density, and the ideal case used has no impact on the data since the model developed here is a semi-empirical fit to actual data.

- One year was assumed (Section 6) to be 8766 hours (24*365.25) for converting times to be more readily used for performance assessment.

- It was assumed that all fuel oxidizes to a plateau at an O/M of 2.40. Most fuels actually oxidize to a plateau slightly higher than 2.40 (Section 6.1.1) and would, therefore, take longer to completely oxidize to the plateau. Thus, this assumption is conservative except for the low-burnup fuels and the high burnup fuels that appear to have released volatile fission products during the oxidation process. This assumption affects the assumed densities, volume expansion coefficients (z_1 and z_2), and Δ(O/M) values used to calculate the extent of reaction, which are used to calculate the pre-exponential factors (Section 6.)

6. ANALYSIS/MODEL

A literature review of the burnup dependence of CSNF oxidation and the effects of moisture on the oxidation process is presented to support the findings from the TGA data. The data used to develop the model parameters are presented, including the literature data for properties of Zircaloy and of the various oxidation states of the fuel. The limited literature data available where the incubation times and unzipping velocities of Zircaloy cladding due to fuel oxidation were measured are given for comparison with the results of the analysis. The model for incubation time and clad unzipping velocity is then developed, with tables of calculated incubation times and unzipping velocities presented for use in performance assessment.

6.1 DATA DEVELOPMENT

6.1.1 Summary of Dry-Air Oxidation Data

The oxidation of both unirradiated UO_2 and CSNF has been studied extensively for over 40 years. Detailed reviews of oxidation testing are found in Hanson (1998), and McEachern and Taylor (1998). These reviews emphasize that unirradiated UO_2 and CSNF oxidize via different mechanisms and at different rates. Data obtained on unirradiated samples, therefore, may not always be directly applicable to repository design.

CSNF with burnup greater than 42 MWd/kgM has been shown to oxidize via the two-step reaction

$$UO_2 \rightarrow U_4O_{9+x} \rightarrow U_3O_8 \qquad \text{(Eq. 1)}$$

Unlike unirradiated UO_2, which is characterized by a surface reaction, CSNF exhibits rapid oxidation of the grain boundaries facilitated by the relatively rapid transport of oxygen through the closely spaced fission-gas bubbles that form on the grain boundaries. This grain boundary oxidation phenomenon is believed to be the reason that CSNF oxidizes at an initial rate a factor of 2 to 50 greater than unirradiated fuel under similar conditions (Novak et al. 1983, p. 264). As oxidation of the grain boundaries and individual grains proceeds, the grains contract as the higher density U_4O_9-like phase is formed, further promoting oxygen transport through the grain boundaries. The U_4O_9 structure formed as CSNF oxidizes accommodates excess oxygen, resulting in a hyperstoichiometric phase with an oxygen-to-metal (O/M) ratio of ~2.4 rather than the nominal value of 2.25. The $UO_{2.4}$ phase then grows into the UO_2 grains by means of oxygen diffusion through the product layer until the entire grain has been converted. No higher oxides, such as U_3O_7 or U_3O_8, have been observed in CSNF oxidized at temperatures up to 195°C until conversion to $UO_{2.4}$ is complete (Einziger et al. 1992, p. 57). As a result of being diffusion controlled, the transition from UO_2 to $UO_{2.4}$ is both strongly temperature and grain-size dependent (Hanson 1998; Stout and Leider 1998, Section 3.2.2.3), with smaller-grained fuels oxidizing faster in accordance with the larger surface-to-volume ratio (Einziger et al. 1991, p. 391).

After oxidation to a nominal O/M ratio of about 2.4, CSNF has shown a resistance to further oxidation exhibited as a plateau on a plot of the O/M ratio as a function of time. Given long enough times or higher temperatures, oxidation to U_3O_8 then proceeds to completion at a nominal O/M ratio of about 2.75. This final phase is also slightly hyperstoichiometric, the O/M ratio of stoichiometric U_3O_8 being 2.67. The plateau behavior has been shown to be strongly temperature, grain-size, and burnup dependent (Hanson 1998, Section 5.2.3; Stout and Leider 1998, Section 3.2.2). These same dependencies are found as the CSNF oxidizes past the plateau to form U_3O_8 (Hanson 1998, Sections 5.2.3 and 5.2.4).

Additional literature evidence (e.g., Choi et al. 1996 and Thomas et al. 1993) for the burnup dependence of the $UO_{2.4}$ to U_3O_8 transition is presented in Hanson (1998, Sections 2.2.2 through 2.2.4) and McEachern and Taylor (1998, Sections 2.3 and 4.). A recent report by McEachern et al. (1998) also indicates that neodymium doping in unirradiated UO_2 tends to inhibit U_3O_8 formation. They oxidized samples over the temperature range 200°C to 325°C for periods of 1 to 5000 hours. The authors (McEachern et al. 1998, p. 147) report an approximately linear relationship between the activation energy for U_3O_8 formation and neodymium content of the doped UO_2:

$$E_{act} = 166 \text{ kJ mol}^{-1} + 5.46x, \qquad \text{(Eq. 2)}$$

where x is the neodymium concentration of the $(U,Nd)O_2$ in atom%. While not identical to the expression reported in Hanson (1998) for CSNF containing a myriad of soluble fission products, the equations are similar and of the same order of magnitude. Further discussion of the burnup dependence of CSNF oxidation is presented with the analysis of the data in Section 6.4.1.

The original interpretation (Hanson 1998) of the oxidation data from TGA tests performed on CSNF fragments did not examine the dependence on grain size because the majority of samples came from the same source and grain size differences were thought to be negligible among those samples. The previous analysis also did not account for the presence of hydrated phases, which are now hypothesized to accelerate the dry-air oxidation process by increasing the effective surface area for absorption of oxygen (Kansa et al. 1998). The data from Hanson (1998) are re-examined in this analysis report, allowing for the effects of possible grain size variations and the presence of hydrated phases. The temperature dependence of the oxidation process is clearly shown and the Arrhenius activation energies to be used in this analysis are derived.

Oxidation of CSNF has exhibited a variety of behaviors. Some samples exhibit plateaus with a nearly-zero slope for extended periods; others exhibit plateaus characterized by a very slow, continual increase in the O/M ratio; and other samples have no observable plateau whatsoever. As a way to provide a rational and consistent basis to analyze the data, Hanson (1998, p. 5.1) proposed defining the O/M ratio at which the plateau occurs, $(O/M)_\delta$, as the O/M ratio at which a local minimum in the time-rate-of-change in the O/M ratio was reached. Further, the duration of the plateau, t_δ, was defined as the time required to oxidize the sample through the range $(O/M)_\delta \pm 0.005$. The time to reach the plateau, $t_{2.4}$, was defined as the time required to oxidize the sample to an O/M ratio of $(O/M)_\delta - 0.005$. It is important to stress that $t_{2.4}$ and t_δ do not necessarily correspond to parameters that are quantitative measures of the state of the fuel or characteristics of the underlying oxidation mechanism. For example, using this methodology,

the range of $(O/M)_\delta$ observed in the TGA tests was 2.35 to 2.43. However, when the low-burnup, smaller-grained samples and the gadolinia-doped samples are excluded, this range is only 2.39 to 2.43. This methodology does not attempt to explain these differences. Using these definitions, the data (DTN: LL000314651021.132) used directly in this analysis to calculate the parameters for the model are given in Table 1 and Table 2. It should again be made clear that any grain size effects would be observed in the time to oxidize a sample from one O/M to another, but these effects are not explicitly determined for the present analysis.

Table 1. TGA Data for the UO_2 to $UO_{2.4}$ Transition

Sample Identification	Oxidation Temperature (°C)	$(O/M)_\delta$	Time to Oxidize $UO_{2.30} \rightarrow UO_{2.35}$ (h)	Time to Plateau[a], $t_{2.4}$ (h)	Average d(O/M)/dt $t_0 \rightarrow t_{30}$ (h^{-1})[b]
105-01	283	2.40	6	55	1.36×10^{-2}
105-02	325	2.39	1.5	7	2.40×10^{-2}
105-03	305	2.39	2.5	17	1.46×10^{-2}
105-04	270	2.40	23	152	5.84×10^{-3}
105-05	255	2.41	30	212	8.09×10^{-3}
105-06	283	2.43	7	161	1.23×10^{-2}
105-07	283	2.41	10	107	8.92×10^{-3}
105-08	283	2.43	17	351	1.47×10^{-2}
105-09	305	2.40	5	46	1.38×10^{-2}
105-10	305	2.41	3	27	1.42×10^{-2}
105-11	305	2.39	5	34	1.35×10^{-2}
105-12	305	2.40	5	43	1.37×10^{-2}
105-13	305	2.40	4.5	32	1.40×10^{-2}
105-14	305	2.42	4	46	1.50×10^{-2}
105-15	305	2.40	2.5	15	2.10×10^{-2}
105-16	305	2.38	3	14	2.13×10^{-2}
105-17	305	2.35	2	10	2.27×10^{-2}
105-18	305	2.39	1	8	2.29×10^{-2}
104-01	305	2.41	3	103	1.37×10^{-2}
104-02	305	2.41	3.5	96	1.31×10^{-2}

DTN: LL000314651021.132

NOTES: [a] $t_{2.4}$ is the time to oxidize from (O/M)=2.00 to $(O/M)_\delta - 0.005$.
[b] Average of hourly d(O/M)/dt taken from time t=0 to t=30 hours

Table 2. TGA Data for the $UO_{2.4}$ to $UO_{2.75}$ Transition

Sample ID #	Oxidation Temp. (°C)	Burnup (MWd/kg M)	Time on Plateau[c], t_δ (h)	Time to Oxidize $UO_{2.45} \rightarrow UO_{2.50}$ (h)	Time to Oxidize $UO_{2.54} \rightarrow UO_{2.59}$ (h)	Time to Oxidize $UO_{2.4} \rightarrow UO_{2.75}$[d] (h)
105-01	283	a	40	35	38	585
105-02	325	a	0.5	2.5	2.8	78
105-03	305	28.1	3.5	6	5.5	112
105-04	270	27.5	788	326	438	b
105-05	255	29.2	300≤	b	b	b
105-06	283	31.5	200	b	b	b
105-07	283	27.6	158	95	97	b
105-08	283	32.5	>3300	b	b	b
105-09	305	a	34	b	b	b
105-10	305	29.8	14	30	37	b
105-11	305	25.9	53	48	61	674
105-12	305	27.9	31	45	47	585
105-13	305	28.3	22	43	60	611
105-14	305	28.1	35	31	37	513
105-15	305	19.1	0.6	3	3	64
105-16	305	18.3	0.8	2.5	3	89
105-17	305	16.7	0.4	1.7	2	21
105-18	305	16.8	0.3	1.2	1	16
104-01	305	42.3	410	382	b	b
104-02	305	42.4	610	b	b	b

DTN: LL000314651021.132

NOTES: [a] Burnup was not measured but should be ~28 MWd/kg M. (See Guenther et al. 1991b).
[b] Not determined–test terminated prior to this point or problems with the data or interpretation of the data.
[c] t_δ = time from $(O/M)_\delta - 0.005$ to $(O/M)_\delta + 0.005$
[d] $UO_{2.75}$ is representative of the final O/M ratio, the actual O/M may be larger or smaller.

6.1.2 Volume Changes Due to Oxidation

Table 3 summarizes the theoretical density and molecular weight for the phases of interest during the oxidation of CSNF. The difference in molecular weight due to variable ^{235}U content and the replacement of uranium ions with fission products or higher actinides has been ignored. It is assumed that the molecular weight of uranium is 238 g mol^{-1} and of oxygen is 16 g mol^{-1}. Given the assumptions for the densities of the $UO_{2.4}$ and $UO_{2.75}$ phases that actually form, the observed variability in the O/M ratio of the product phases, and the variable molecular weight due to fission products and higher actinides, the assumptions for the molecular weight of uranium and oxygen introduce negligible uncertainty.

Table 3. Characteristics of Fuel Phases of Interest

Phase	Density[a] ($g\ cm^{-3}$)	Molecular Weight ($g\ mol^{-1}$)	Volume ($cm^3\ mol^{-1}$ U)[c]	Volume relative to UO_2
UO_2	10.96	270	24.635	1.0000
U_4O_9	11.30	1096	24.248	0.9843
$UO_{2.4}$	11.30[b]	276.4	24.460	0.9929
U_3O_7	11.40	826	24.152	0.9804
U_3O_8	8.35	842	33.613	1.3644
$UO_{2.75}$	8.35[b]	282	33.772	1.3709

NOTES: [a] Density data as documented in Table 2.1 of Hanson 1998.
[b] Density assumed to be that of the similar stoichiometric phase.
[c] Calculated using volume = molecular weight/(density×number of moles U in the phase).

The change in volume resulting from oxidation can not be calculated by simply taking the ratio of the densities for the phases involved; this method neglects the change in mass of the fuel that accompanies the uptake of oxygen. Volume changes need to be calculated by taking the ratio of the phase volumes on a per mole uranium basis. From Table 3, it can be shown that the nominal contraction of UO_2 as it oxidizes to form U_3O_7 or U_4O_9 is ~2%. However, the calculated volume contraction for formation of $UO_{2.4}$ in CSNF is only ~0.7%, assuming the same theoretical density as the stoichiometric U_4O_9. The volume contraction is actually much larger, ~9%, if an initial density of 92% of the theoretical density is used, and it is assumed that the density of the oxidized phase approaches its theoretical density. It is clear that the oxidation of UO_2 to $UO_{2.4}$ can result in a volume contraction in the range 0.7% to about 9%. The slight densification of the fuel has been shown (Thomas et al. 1993, p. 312; Thomas and Einziger 1992, pp. 150-152) to result in cracking of the oxidized grains. Such cracking probably occurs only with larger volume contractions. However, in order to maintain a conservative approach to clad unzipping due to fuel oxidation, the volume contraction of 0.7% shall be used in this analysis.

As the fuel continues to oxidize, the less dense U_3O_8 phase forms. The volume expansion of U_3O_8 relative to the original UO_2 is 36% as is often reported in literature (e.g., Taylor et al. 1993, p. 164). This expansion is slightly higher, 37%, if the hyperstoichiometric $UO_{2.75}$ is formed and it is assumed that the theoretical density of the $UO_{2.75}$ is the same as for the stoichiometric U_3O_8. It is this large volume expansion upon formation of U_3O_8 that can stress the cladding and result in unzipping. The volume expansion can be significantly less, ~26%, if an initial density of 92% of theoretical density of the UO_2 is used, and it is assumed that the $UO_{2.75}$ formed approaches its theoretical density. Again, to maintain a conservative approach, a total volume expansion of

37% from the original UO_2, or 38% from the $UO_{2.4}$ phase that forms as an intermediate, was used in this analysis.

6.1.3 Fuel Rod Characterization

The fuels used in the TGA and dry-bath oxidation tests have all been characterized to determine the properties of the fuel, both pre- and post-irradiation. Of importance to this analysis are such properties as the fuel grain size, burnup, diameter of the fuel pellets and cladding, and the nominal active fuel length in a rod. Table 4 summarizes these properties as described in each of the references cited. These data are used as guidance to provide typical values. They are not used directly in the calculation of the model parameters, but are used for calculation of the unzipping velocities in Section 6.6.

Table 4. Approved Test Material (ATM) Fuel Characteristics

	ATM-103	ATM-104	ATM-105	ATM-106	Turkey Point
Reference	Guenther et al. 1988a	Guenther et al. 1991a	Guenther et al 1991b	Guenther et al. 1988b	Davis and Pasupathi 1981
Reactor Type	PWR	PWR	BWR	PWR	PWR
Fuel Type	CE 14×14	CE 14×14	GE 7×7	CE 14×14	W 15×15
Post-irradiation Grain Size					
Low-burnup region (μm)	16.3-18.7	11.0-11.6	11.3-12.4	6.4-7.5	20-30 (ave)
High-burnup region (μm)	16.3-21.7	9.6-13.7	11.3-15.4	6.6-16.2	
Nominal Burnup Range (MWd/kgM)	13-33	20-44	18-34	27-47	20-28
Pre-irradiation Diameters (cm)					
Fuel (outside)	0.9563	0.9563	1.21	0.9639	N/A
Cladding (inside)	0.9855	0.9855	1.242	0.986	0.948
Nominal Active Fuel Length (cm)	347.2	347.2	371	347.2	365.8

It should be noted that the fuel grain sizes are determined using a linear intercept method. The number reported is thus an average for several measurements. The measured grain size was multiplied by a correction factor of 1.57 to obtain the true grain size. This factor was derived using an initial log-normal distribution of grain sizes (Mendelson 1969, p. 446). Grains are also subjected to various degrees of grain growth depending on the temperature distribution the fuel experiences. An individual sample is thus composed of a log-normal distribution of grain sizes about the mean reported in Table 4, with a broadening of the distribution peak to both the larger and smaller sizes if significant grain growth has occurred.

From Table 4 it is clear that as-fabricated fuel/clad radial gap sizes are on the order of 100 to 150 μm. However, during the irradiation process the fuel undergoes an initial densification stage at relatively low burnups. The fuel then begins to swell with increasing burnup due to the accumulation of point defects and fission gases. At the same time, the cladding undergoes creep, depending on the pressurization of the fuel rod, that could reduce the fuel/clad gap. Thermal cycling also causes cracking of the fuel pellets, which also results in closure of the gap. The

final gap is thus strongly dependent on the reactor operating conditions as well as the initial gap size. To maintain a conservative approach without requiring additional experimental or modeling work, this analysis assumes that the fuel/clad gap upon emplacement in the repository is zero; that is, the fuel is touching the cladding. The derivation of the model will allow a gap size to be included, however.

6.1.4 Properties of Zircaloy

As will be shown in Section 6.6, the yield stress, σ_{yield}, and the elastic shear modulus, G, of the cladding are needed to calculate the unzipping velocity once a crack has been initiated. The shear modulus, in turn, is derived form the Young's modulus, E, and Poisson ratio, ν, of the Zircaloy by the expression (Dieter 1961, p. 38)

$$G(T) = E(T)/2(1+\nu(T)) \qquad \text{(Eq. 3)}$$

The yield stress is also a function of temperature. Table 5 lists the properties for unirradiated Zircaloy-2 from Table A.6 of Glasstone and Sesonske (1994, p. 486)

Table 5. Properties of Unirradiated Zircaloy-2

Temperature (K)	Yield Strength (MPa)	Young's Modulus (MPa)	Poisson's Ratio
300	300	95000	0.43
500	170	90000	0.38
600	117	78000	-

Irradiation is known to dramatically change some of the properties of the Zircaloy. The irradiation embrittlement of the Zircaloy due to bombardment with neutrons is equivalent to cold working. It is expected that the yield strength would increase with the total neutron fluence. Since the burnup of the fuel is directly related to the total neutron fluence, the properties of Zircaloy can be expected to exhibit a dependence related to burnup. CRWMS M&O (1998, p. 13) used a yield strength of 780 MPa at 25°C in the analysis, a factor of about 2.6 larger than for unirradiated cladding. The values of Young's modulus are also expected to increase with burnup, but the changes are minimal compared with the changes to the yield stress. The values for Poisson's ratio are not expected to change much due to irradiation although the values listed in Table 5 seem a little large. (An isotropic material has a theoretical value ν=0.33 [Dieter 1961, p. 36].)

Since it will be shown in Section 6.6 that the unzipping velocity is a function of G/σ_{yield}, it holds that the unzipping velocity will be conservative, i.e., faster than might be expected, for larger values of G and E, and for smaller values of ν and σ_{yield}. Given this approach, and the uncertainty about whether the irradiated properties will change over extended periods at elevated temperatures (i.e., annealing effects), for the basis of this analysis the unirradiated properties will be used. The resulting unzipping velocities will be faster, and, thus, conservative by a factor of between 2 and 3 than if the irradiated properties are used. The effect will be especially pronounced at lower temperatures.

The temperature-dependent Young's modulus, yield strength, and Poisson's ratio are thus derived as a function of temperature (K) to fit the data in Table 5 to obtain the following equations:

$$E(T) = 98639 - 8.94489\times10^{-5} \times T^3 \quad \text{MPa} \qquad \text{(Eq. 4)}$$

$$\sigma_{yield}(T) = 483 - 0.6157 \times T \quad \text{MPa} \qquad \text{(Eq. 5)}$$

$$\nu(T) = 0.505 - 2.5\times10^{-4} \times T \qquad \text{(Eq. 6)}$$

6.1.5 Effect of Variable Moisture Content on Oxidation

6.1.5.1 During Oxidation

The introduction of water complicates the oxidation process by facilitating formation of hydrated oxidation products. The analysis of CSNF interactions with direct water contact and with saturated vapor is not considered part of the dry unzipping model. However, the effect of variable moisture content (i.e., in the range 0% to 100% relative humidity) may be important to "dry" oxidation and clad unzipping.

While there have been various experiments performed to determine the effect of moisture on oxidation of UO_2 and CSNF, the results are not clear and are often contradictory. Woodley et al. (1989, pp. 74, 87) performed TGA testing on CSNF samples over the temperature range 140°C to 225°C and varied the nominal dewpoint from –70°C to +14.5°C. They concluded that the variation in moisture content had little measurable effect on the oxidation rate, and, if anything, oxidation was somewhat faster in dry air. Einziger et al. (1991, pp. 389-391) also examined oven dry-bath CSNF oxidation over the temperature range 110°C to 175°C and at nominal dewpoints of -55°C or +80°C. Again, the effect of moisture on the oxidation from UO_2 to U_4O_9 was found to be minimal; however, oxidation was found to be somewhat faster in moist air. They also report that the effect is more pronounced for both lower temperatures and for the boiling water reactor (BWR) fuel tested, and that the effect is greater at higher O/M ratios. No hydrated phases were reported for either series of tests.

Taylor et al. (1989) studied the oxidation of UO_2 in air-steam mixtures at 200°C and 225°C. They report (Taylor et al. 1989, p. 72) measurable UO_3 hydrate formation within 20 days at 200°C and 5 days at 225°C. More importantly, they found that below ~50% saturation, the rates and products of UO_2 oxidation are the same as for dry-air oxidation (Taylor et al. 1989, p. 72). Above ~50% saturation, UO_3 hydrated phases, primarily dehydrated schoepite ($UO_3 \bullet 0.8\ H_2O$) and schoepite ($UO_3 \bullet 2\ H_2O$), were observed (Taylor et al. 1989, p. 72). With water in excess of saturation so that the specimens were fully wetted, much larger crystals of dehydrated schoepite were obtained (Taylor et al. 1989, p. 73). The relative humidities in the work of Woodley et al. (1989) and Einziger et al. (1991) were well below the ~50% saturation level, and this could explain why no significant effect was observed. Below this threshold limit, there does not appear to be sufficient moisture to form a stable water film on the fuel surface that is necessary

to provide a medium for uranium to dissolve and reprecipitate as a hydrate (Taylor et al. 1989, pp. 74-75).

Sunder and Miller (1996) also studied oxidation of unirradiated UO_2 at 150°C with an applied gamma radiation field. They confirmed formation of U_3O_8 within about two years on all samples exposed to air or O_2 in the applied gamma field (Sunder and Miller 1996, p. 128). The samples exposed to O_2 and 60% saturated steam underwent the most extensive oxidation (Sunder and Miller 1996, p. 129). Both hydrated phases and U_3O_8 were formed during the oxidation. However, virtually no oxidation occurred for samples exposed to Ar and 60% saturated steam (Sunder and Miller 1996, p. 129). Such a finding is not unexpected, as UO_2 is relatively benign in reaction with steam in the absence of oxygen.

Defected CANDU (Canada deuterium) spent fuel has also been studied to determine the effect of moisture on oxidation (Wasywich et al. 1993, Johnson and Taylor 1998). In these tests, spent fuel elements with small cladding defects were exposed to aerated steam at 150°C in five different experimental phases totaling almost 9.5 years. The initial ~7.75 years were at limited oxygen concentrations; therefore, the results must be interpreted with caution. For example, the oxygen concentration during the 720-day interval of Phase 4 showed a decrease in oxygen from the original 20% to less than 0.28% (Johnson and Taylor 1998, Section 3.1). During Phase 5 (dry air), it was found that the oxygen concentration dropped by a factor of ~2 within 25 days. Thus, the oxygen availability during most of the testing was very low and most likely greatly limited the extent of oxidation. Since oxygen depletion occurred for both the moist- and dry-air experiments, however, the differences in behavior observed may be attributed to the presence of moisture.

In the dry-air experiments, Wasywich et al. (1993) found behavior comparable to other oxidation studies on CANDU spent fuel. That is, oxidation beginning wherever the oxygen had direct access to the UO_2 surfaces, followed by preferential grain boundary oxidation. The U_3O_7-like phase then grew into the individual grains until conversion was complete. The behavior of the samples exposed to a moist-air environment was quite different, with alteration occurring throughout the length of the fuel element rather than being localized to the defect region. Possibly because of the limited oxygen supply, bulk oxidation of grains was absent in the moist-air tests. It is important to note that at the end of the additional 660-day oxidation of Phase 5, where the oxygen supply was replenished to maintain full aeration, extensive bulk oxidation of individual grains to U_4O_9/U_3O_7 and formation of significant amounts of UO_3 hydrate occurred (Johnson and Taylor 1998, Section 4.4.3.2)

The effect of moist air on CSNF, however, is not clear. The rapid grain boundary oxidation observed in the CANDU fuel is already characteristic of CSNF oxidation. This, in addition to the low relative humidities in the tests of Woodley et al. (1989) and Einziger et al. (1991), may explain why moisture is reported to have only a limited effect on oxidation of CSNF. Neither of these studies have examined the effect of moisture over long enough periods to determine the direct effect of moist air on the U_4O_9 to U_3O_8 transition. Thus, the effect of moist air at relative humdities between about 50% and 100% on CSNF oxidation especially for the U_4O_9 to U_3O_8 transition, is not sufficiently understood.

6.1.5.2 Prior to Oxidation

Fuel in rods that fail during reactor service may be subjected to steam oxidation. Recent work by Olander et al. (1999, p. 18) has shown that in-reactor steam oxidation, accounting for thermal oxidation, reaction in the interior of cracked pellets, and steam radiolysis should not theoretically drive the O/M ratio above ~2.008 because of limitations imposed by the presence of hydrogen. However, post-irradiation examination of some failed fuels has revealed radially averaged O/M ratios as high as ~2.06 (Olander et al. 1999, p. 12). During the depressurization and cooling of the reactor prior to shut down, failed fuel rods may fill with reactor coolant water. Water ingress is also possible during storage in the spent fuel storage pools. Olander et al. (1999, p. 18) speculate that reaction with water, not steam, may result in the observed oxidation of the fuel above the predicted limits.

Kohli et al. (1985) performed oxidation studies on two BWR fuel elements that had failed during reactor operation and then had been placed in pool storage for ~4 years before being sent to a hot cell facility for examination and testing. They report that not all water was removed from the rods by subjecting them to a vacuum; rather, some water continued to be released as the fuel was heated, both under vacuum and during the oxidation test. They did not report the presence of hydrated phases, either in pre- or post-test examination. However, they did report that X-ray diffraction (XRD) of fuel samples taken before testing showed that the fuel had an O/M ratio of 2.33, with the tetragonal doublets of the U_3O_7 being clearly resolved (Kohli et al. 1985, pp. 192, 196). Just as important, XRD of fuel samples taken after oxidation testing showed (Kohli et al. 1985, pp. 192, 196) the fuel to be best fit to reference data of a $UO_{2.9}$ phase, as opposed to the U_3O_8 observed during dry-air oxidation. It is not clear from the published reports from where the XRD samples were taken or how extensive this oxidation might have been. The assembly average burnup for this fuel was 17.2 MWd/kg U (Kohli et al. 1985, p. 187); the actual average burnup of this rod could be higher or lower. Nevertheless, it is unclear at what burnup the fuel matrix is stabilized such that U_4O_9 (maintaining the cubic structure of UO_2) is formed as opposed to the U_3O_7 phase reported for unirradiated UO_2, CANDU spent fuels with burnups lower than typical CSNF, and the BWR fuel tested here. At what point the oxidation of the fuel occurred is unknown, but oxidation at the relatively low temperatures of spent fuel pools should proceed quite slowly. However, it is clear that some failed rods may have at least portions of the fuel at oxidation states higher than 2.00 upon emplacement.

As described in Hanson (1998, Section 5.3), there is an apparent contradiction between the oxidation data obtained using TGA and data obtained from the oven dry-bath apparatus. At 175°C, 195°C, and 255°C, the dry-bath samples exhibited shorter plateaus than were predicted based on extrapolation of TGA data to the lower temperatures. EPRI (1986, Figure 3-1) had reported the duration of the plateau to be approximately 10^4 hours for bare fuel oxidized at 250°C. Hanson (1998, p. 5.36) reported a plateau of 10^4 hours was expected based on extrapolation of the TGA data. For each of the ATMs tested, the longest plateau actually observed in the 255°C dry-bath tests using fuel that had not been pre-oxidized at lower temperatures was only about 2000 hours, a factor of 5 shorter than expected. While the exact cause of this apparent discrepancy is not known, it seems likely that the presence of moisture plays a significant role. All dry-bath samples were exposed to the ambient atmosphere of the hot cell during any interim weighings. The exposure to moisture from those tests using humidified

air may have accelerated surface oxidation. XRD has confirmed the presence of hydrated phases on at least eight of the TGA samples (DTN: LL000314651021.132) with at least three of the samples having more than just a trace quantity. When duplicate samples were tested from the same original fragment, only some indicated the presence of the hydrated phases. Thus, it seems that the hydrated phase is only a minor component of the total sample, and the small (~5 mg) sample taken for XRD analysis may not be sufficiently representative of the original fragment (~200 mg) to absolutely determine whether a hydrated phase is present. Scanning electron microscopy (SEM) examination of some TGA samples (DTN: LL000314651021.132) has identified needlelike structures, possibly hydrated phases, on some of the oxidized particles. In all cases, it appears that these needles exist only on one face of the particle.

It has been hypothesized that the hydrated phase formed on the surface of the fragments prior to oxidation testing in either the TGA or oven dry-baths. As reported by McEachern and Taylor (1998, p. 92), a few studies have indeed identified UO_3 and its hydrates forming on UO_2 under ambient conditions. The samples with the hydrated phase usually exhibited a relatively fast, nonlinear weight gain at early times after the plateau in the TGA tests. At first it was hypothesized (Kansa et al. 1998) that these samples contained an unusually high fraction of fine grains due to fabrication, irradiation, or subsequent cracking during the oxidation process. Such a large number of fine grains was not supported by SEM photomicrographs of these samples. It was thus hypothesized (Kansa et al. 1998) that the presence of hydrated phases on the surface of CSNF grains acted as "fins" that could greatly enhance the effective surface area. This is equivalent to decreasing the effective grain size of the sample. Not only could the large surface area created by the needlelike hydrated phase allow for greater oxygen absorption, but the low-density, highly oxidized material could rapidly transport this oxygen to the U_4O_9 phase beneath it. If this were the case, the effect from the "fins" should decrease as more of the fuel oxidizes to U_3O_8 and cracks or spalls from the surface. This is observed with the TGA samples that exhibited this accelerated oxidation process; after some initial transient after the plateau, the oxidation proceeds in a manner similar to that of the other samples. Using this justification, the effective grain size was reduced for these samples and the fit with the oxidation model developed in the Waste Form Characteristics Report (Stout and Leider 1998, Section 3.2.2.10) was quite good.

The effect of moisture on oxidation of CSNF may be significant, during both the oxidation process and if the fuel reacted with water to form hydrated phases prior to oxidation. Since most of the failed fuel emplaced in the repository will have experienced failure during reactor operation, the effect of moisture and/or hydrated phases may be important and may affect the assumed starting O/M ratio (e.g., Kohli et al. 1985, p. 192 and 196).

6.1.6 Summary of Clad Unzipping Experiments from Literature

Oxidation studies on bare fuel have been performed to determine the kinetics and mechanisms of spent fuel oxidation. These studies are useful only if the data can be used to predict the unzipping behavior of defected fuel rods. Only a limited number of experiments on defected rods have been performed, none of which were part of this experimental program. Table 6 summarizes these experiments.

Table 6. Incubation Times and Unzipping Velocities from Literature

Reference	Temperature (°C)	Burnup (MWd/kg M)	Incubation Time (h)	Unzipping Velocity (cm min^{-1})
Novak	250	0[a]	~600	b
Novak	250	0	>942	b
Boase	300	0	4<t<7	1.2×10^{-4}
Novak	230	7.1	~601	b
Novak	230	7.9	b	2.3×10^{-5}
Novak	250	7.9	118<t<208	1.2×10^{-4}
Boase	250	8.2	b	$\sim1\times10^{-4}$
Kohli[c]	325	17.2	<<2100	$<1.9\times10^{-4}$
Einziger ('85)	229	<11.9	~1000	$<3\times10^{-5}$
Olsen	217-230	~11.9	<<7206	b
EPRI ('86)	295	36	>1676	b
EPRI ('86)	360	~27	20	2.3×10^{-3}
EPRI ('86)	360	~27	52<t<60	$>1.7\times10^{-3}$
EPRI ('86)	325	~27	79	1.4×10^{-3}
EPRI ('86)	325	~27	455	1.4×10^{-3}
EPRI ('86)	295	~16	55<t<131	$>1.2\times10^{-3}$
EPRI ('86)	295	~21	>80	1.0×10^{-3}
EPRI ('86)	295	~27	131<t<232	$>9.8\times10^{-4}$
EPRI ('86)	295	~27	386<t<551	$>4.4\times10^{-4}$
EPRI ('86)	283	~8	~40	1.0×10^{-3}
EPRI ('86)	283	~27	1125	4.8×10^{-4}
EPRI ('86)	283	~21	~210	4.0×10^{-4}
EPRI ('86)	283	~27	830	3.0×10^{-4}
EPRI ('86)	250	~27	~5000	b
EPRI ('86)	250	~27	9754<t<10545	b
EPRI ('86)	250	~27	>10545	b
Nakamura	200	~14	>11,200	b
Nakamura	220	~15.7	~4000	b
Nakamura	240	~26.6	~1000	b

NOTES: The references correspond to Novak et al. (1983), Boase and Vandergraaf (1977), Kohli et al. (1985), Einziger and Cook (1985), Olsen (1985), EPRI (1986), and Nakamura et al (1995).

[a] This test was on stainless steel cladding.
[b] Not calculated or not reported.
[c] Limited air greatly reduced the oxidation rate.

6.1.6.1 Unirradiated UO_2

Early work referenced by Novak et al. (1983, p. 254) showed that unirradiated UO_2 elements in deliberately defected stainless steel cladding exhibited swelling and clad failure at ~600 hours when oxidized at 250°C. There was no detectable weight gain during the two-month experiment at 175°C. Novak et al. (1983) conducted oxidation tests on unirradiated, defected CANDU fuel

elements at 230°C and on mini-elements at 250°C. Unlike the referenced work where the elements had a single, intentional defect, the work of Novak et al. (1983) was performed on elements with one, four, and six defects. Even with four defects, the unirradiated mini-element showed no signs of splitting even after 942 hours at 250°C (Novak et al. 1983, p. 263). Obviously, the different properties of the cladding material, i.e., Zircaloy vs. stainless steel, are important. However, it is clear that significant quantities of U_3O_8 formed in the referenced sample for clad failure to occur. It is not clear why oxidation of that sample proceeded much more rapidly than observed for other samples oxidized at 250°C. Novak et al. (1983, Figure 12a) reported that the weight gain for the unirradiated elements oxidized at 230°C was minimal over the 600 hours tested.

Boase and Vandergraaf (1977) oxidized unirradiated, defected CANDU elements at 300°C. They reported longitudinal crack development from a circular defect after ~7 hours, and in less than 4 hours for slit defects (Boase and Vandergraaf 1977, p. 68). The oxidation front was well defined, with little oxidation in the fuel/clad gap ahead of the front. An average value for the linear velocity of the oxide front was calculated as 1.2×10^{-4} cm min^{-1} at 300°C, in close agreement with their calculated value of 3×10^{-4} cm min^{-1} for unclad pellets (Boase and Vandergraaf 1977, p. 68). Below 300°C, Boase and Vandergraaf (1977, Fig. 14, p. 70) report an Arrhenius temperature dependence for the velocity of the oxide front with an activation energy of 170 kJ mol^{-1}. At 200°C, the velocity of the oxidation front is thus predicted to be approximately 10^{-7} cm min^{-1} (Boase and Vandergraaf 1977, p. 68).

6.1.6.2 Irradiated Fuel

Novak et al. (1983) oxidized CANDU fuel elements with deliberately defected cladding, either one or six defects, at 220°C, 230°C, and 250°C for up to 685 hours. For elements with an approximate burnup of 7.1 MWd/kg U and a typical grain size of 10 μm, there was no significant diametral change for either defect case at 220°C although weight increase was clearly observed (Novak et al. 1983, p. 257). After 601 hours at 230°C, there was a maximum diametral increase of ~1% in the central region of the fuel element where four of the defects were located (Novak et al. 1983, p. 257). It appears that a crack was just beginning to form at one of the defects (Novak et al. 1983, Figure 4b, p. 257). At each end, where one defect was made, there was no significant diametral increase, although there was extensive oxidation to the U_3O_7 or U_4O_9 phase with measured O/U values between 2.35 and 2.38 (Novak et al. 1983, p. 258). Measured O/U ratios in a region intermediate between the one- and four-defect regions were 2.01 (Novak et al. 1983, p. 258).

Novak et al. (1983) repeated the experiments using a fuel with a slightly higher burnup of approximately 7.9 MWd/kg U and similar grain size. At 220°C and 230°C, the behavior was similar to the lower burnup fuel although a close examination of the data reveals that the higher burnup fuel appears to be oxidizing at a slightly slower rate. It is important to note that the oxidation rates at 230°C for the irradiated fuels were a factor of 15 to 50 higher than for unirradiated UO_2 (Novak et al. 1983, p. 262). The velocity of the oxidation front was estimated (Novak et al. 1983, p. 263) as 2.3×10^{-5} cm min^{-1}. At 250°C, the maximum diametral increase for an element with one defect was ~2% after 208 hours of oxidation and the element showed

evidence of cracking at the defect (Novak et al. 1983, p. 260). A longitudinal split occurred in the area of four defects, with diametral increases of 5% to 12%, for a six-defect rod of the higher burnup fuel. This split occurred sometime between 118 hours and 208 hours of oxidation at 250°C (Novak et al. 1983, p. 260). At the large split, oxidation is near 100%; however, in the region ~1 cm away, the reported O/U ratio is only 2.1, showing that the oxidation falls off rapidly away from the defect. Oxidation at the single hole of that rod corresponds with an O/U ratio of 2.4, but oxidation again falls off to an O/U ratio of ~2.15 in an adjacent sample (Novak et al. 1983, p. 261). The estimated velocity (Novak et al. 1983, p. 263) of the oxidation front at 250°C is 1.2×10^{-4} cm min^{-1}. Again, it is important to note that the oxidation rate was a factor of at least 2 greater for the irradiated fuel at 250°C than for unirradiated samples. Novak et al. (1983, p. 263) report that a 2% diametral strain is needed for significant splitting of the cladding. However, it appears that cracking can initiate with a strain of less than 1% as reported for the 230°C test (Novak et al. 1983, pp. 257-258).

Boase and Vandergraaf (1977) oxidized intentionally defected CANDU fuel elements with average burnups of 8.2 MWd/kg U at temperatures between 250°C and 370°C. While they do not directly report incubation times, they do report that the irradiated elements showed higher rates of oxidation than the unirradiated elements (e.g., Figure 14). Typically, the irradiated fuel exhibited a velocity of the oxidation front a factor of 10 higher than the unirradiated fuel. At 250°C, the velocity for the irradiated fuel (Figure 14) is approximately 10^{-4} cm min^{-1} and the extrapolated value (Boase and Vandergraaf 1977, p. 68) at 200°C is approximately 1×10^{-6} cm min^{-1}. The oxidation front was also less defined than for the unirradiated elements, and the irradiated elements developed secondary swell areas some distance from the initial defect.

Kohli et al. (1985) studied the oxidation of BWR rods that had failed during reactor operation. Two rods were tested at 325°C, one in an argon environment and the other, a rod from an assembly with an average burnup of 17.2 MWd/kg U, in air. Both rods were subjected to applied heat and vacuum pumping to remove water trapped in the rod. In addition to the defects formed during reactor operation, each rod had an additional defect (~3.0 mm hole) drilled in the plenum to facilitate release of water. The fuel rod tested in argon experienced no further degradation. Significant increases in the defect sizes for the fuel rod tested in air for 2100 hours were measured. However, since the fuel had an O/M ratio of 2.33 (Kohli et al. 1985, p. 192) prior to testing and no interim examinations were performed, an incubation time can not be calculated from this data.

Kohli et al. (1985) report oxide front velocities (p. 197), measured at three different defects, in the range 6.9×10^{-5}cm min^{-1} to 1.9×10^{-4}cm min^{-1}. The fastest velocity is for the defect in the plenum, where the burnup is significantly lower than for the bulk of the rod. No powder formation was found at or beyond 2.5 cm from the end of a crack, again showing that the fuel oxidation is highly localized, at least for the second transition (Kohli et al. 1985, p. 193). The oxide front velocities are about one order of magnitude smaller than those reported above by Novak et al. (1983) and Boase and Vandergraaf (1977, p. 68). This is not expected since the presence of hydrated phases, indicated by the final oxidation state with an O/M ratio of 2.9 (Kohli et al. 1985, p. 192), is hypothesized to accelerate the oxidation process based on the arguments presented earlier with respect to the effect of hydrated phases. However, it is essential to note that the gas in the air capsule was replenished periodically only twice weekly for

the first 1500 hours, then daily or twice daily for the remaining 600 hours (Kohli et al. 1985, p. 190). Oxygen depletion at 325°C would be significant in a matter of hours (Kohli et al. 1985, p. 190, the authors report a ~20% decrease in absolute pressure within 10 hours), so the oxidation was greatly limited over the first 1500 hours and would significantly lower the oxidation front velocity. Kohli et al. (1985, p. 190) state that the total air introduced into the capsule was estimated to be enough to oxidize only ~6% of the fuel. Thus, the lower oxide front velocity must be viewed with great caution when comparing to tests run with unlimited air.

Einziger and Cook (1985) tested intentionally defected and intact pressurized water reactor (PWR) and BWR rods in inert and air atmospheres at 229°C. No breaching of the intact rods occurred over the lifetime of the tests. The precise burnup of the individual rods is not known; however, the reported assembly-average burnup for the BWR fuel was 11.9 MWd/kg M, while the peak burnup for the PWR fuel was 30.9 MWd/kg M (Einziger and Cook 1985, p. 57). Defects (0.76 mm-diameter holes, Einziger and Cook 1985, p. 58) were drilled in the cladding near the fuel midplane and near the top of the fuel column. An interim examination performed after 2235 hours of oxidation showed that a crack 1.13 cm in length had formed at the upper defect of the BWR rod tested in air (Einziger and Cook 1985, Table VI). This crack continued to grow and was 5.51 cm in length when the test was halted after 5962 hours of oxidation (Einziger and Cook 1985, p. 60). It was found that U_3O_8 was present up to about 2.5 cm from the split at the upper end of the rod (Einziger and Cook 1985, Figure 11). Some U_4O_9 was observed at distances approximately 7 cm from the crack. Einziger and Cook (1985, p. 68) report that a 6.5% strain accompanied the section of fuel that had oxidized in front of the crack. They use a 6.5% strain as the value necessary for crack propagation to occur. Using these values, they estimate an incubation time of ~1000 hours and an oxide front velocity of between 2×10^{-5} and 3×10^{-5} cm min^{-1} (Einziger and Cook 1985, p. 69). No degradation of the rods tested in argon or the PWR rod tested in air was reported.

Olsen (1985) reported that even after 5962 hours at 229°C and an additional 7206 hours at temperatures between 217°C and 230°C, no evidence of crack formation in the PWR rods (in inert or air atmosphere) or BWR rod in an inert atmosphere was observed. Post-test analyses of these rods showed that some oxidation of the fuel had occurred due to air leakage into the system although not enough to result in clad unzipping. About six times the axial fuel stack length was attacked in the PWR rod oxidized in air compared with the BWR rod (Olsen 1985, p. 115). It thus appears that the higher activation energy of the $UO_{2.4}$ to $UO_{2.75}$ transition, corresponding to higher burnups, results in a larger area of conversion to $UO_{2.4}$ before U_3O_8 formation begins. One new BWR rod (Olsen 1985, p. 28) was tested in unlimited air for 7206 hours at temperatures decreasing from 230°C to 217°C. The defects at the top and center of the rod may not have penetrated through the wall of the cladding. However, a crack of 1.88 cm formed at the defect near the bottom of the fuel rod (Olsen 1985, p. 28). Average grain sizes (Olsen 1985, p. 29) for the fuel near the defected region range from 5.7 μm to 9 μm. Oxidation up to 13 cm from the defect was reported (Olsen 1985, pp. 28-30).

Einziger and Strain (EPRI 1986, p. 2-2, 2-5) oxidized segments (~20 cm) of Turkey Point fuel with intentional defects induced by pressurizing the segment to ~15 MPa while heating to 325°C (creating breaches ranging from 8 μm to 52 μm effective circular diameter) or by drilling a 760 μm diameter hole. The typical burnup (EPRI 1986, Table 2-2) of the rods tested was ~27

MWd/kg M; however, some segments from the ends of the rods were tested and have lower burnups. The precise burnup of each segment is not known, but even with a relatively flat gamma profile, variations in burnup significant enough to affect oxidation behavior can exist. Oxidation tests were conducted on the Turkey Point fuel at 250°C, 283°C, 295°C, 325°C, and 360°C. One segment of Big Rock Point fuel was also tested at 295°C (EPRI 1986, p. 4-2). This segment, with an approximate burnup of 36 MWd/kg M, displayed only minimal cladding deformation after 1676 hours in contrast with the Turkey Point samples oxidized at 295°C that all exhibited clad splitting within 551 hours. With the exception of the 250°C tests, the 760 μm defect propagated before the smaller defects when samples of similar burnup were compared (EPRI 1986, Table 3-3). This is one possible indication that transport limitations of oxygen to the fuel plays an important role. Still, differences in incubation times in the range of a factor of 1.5 to 5 are readily observed, depending on the temperature and the size of the defects (EPRI 1986, Table 3-3). It is also clear that the samples with lower burnup had incubation times a factor of 2 to 30 less than samples of higher burnup oxidized at the same temperature (EPRI 1986, Tables 2-1 and 3-3). Such samples also had clad unzipping velocities as much as a factor of 3 faster than the higher burnup counterparts.

Of particular interest are the tests at 250°C. The bare fuel samples exhibited plateaus of at least 10^4 hours (EPRI 1986, Figure 3-1), yet two of the cladded segments exhibited incubation times of ~5000 hours and less than 10545 hours, respectively (EPRI 1986, Table 3-3). The third sample had an incubation time of at least 10545 hours. While the type of defect and oxygen-transport limitations play an important role, the smaller defects propagated first at these temperatures. If the crack growth is due to fuel oxidation, this question follows: Why would enough U_3O_8 form to cause crack growth in two of the samples, yet the bare fuel was still on the plateau? Two different factors, burnup and the presence of hydrated phases, may explain this apparent discrepancy. It is possible that differences in sample burnup could result in a wide range of times on the plateau. It was also observed (EPRI 1986, Figure 3-1) that the bare fuel samples at 283°C and 295°C exhibited mass increases greater than the ~4.4% necessary to fully oxidize the samples to U_3O_8. This would suggest that oxides with oxidation states above U_3O_8 were formed, which should only be possible if moisture or hydrated phases were present. X-Ray Diffraction (XRD) of some of the oxidized fuel confirmed the presence of UO_3 or $UO_{2.9}$ for samples oxidized at 250°C, 283°C, and 295°C (EPRI 1986, Table 3-2). Similar variability has been observed for the dry-bath samples oxidized at 255°C (Hanson 1998, Section 4.3.3). The presence of moisture or hydrated phases on some of the samples may account for the much faster times for U_3O_8 formation.

Nakamura et al. (1995) oxidized irradiated and unirradiated rodlets with artificial defects in air and air-argon mixtures at temperatures in between 200°C and 240°C. Clad degradation occurred at 1000 hours for a section of a rod with a burnup of 26.6 MWd/kg U oxidized at 240°C (Nakamura et al. 1995, p. 323). A rodlet with a burnup of 15.7 MWd/kg U oxidized at 220°C required 4000 hours for further degradation (Nakamura et al. 1995, p. 323), while a rodlet with a burnup of 14.0 MWd/kg U displayed swelling, but no breakage even after 11,200 hours at 200°C (Nakamura et al. 1995, Figure 2a). More importantly, the authors report that the bulk O/M ratio for each case was approximately 2.40 (Nakamura et al. 1995, p. 328). This suggests that only small amounts of U_3O_8 are needed to cause clad degradation, as supported by their claim that only a 2% strain was needed to break the cladding at the defect (Nakamura et al. 1995, Figure 3,

p. 331). They also indicate that oxidation of the irradiated rod progressed faster at the center part of the pellet than at the periphery (Nakamura et al. 1995, p. 327), thus supporting the radial burnup dependence of Hanson (1998, Section 2.3.2). Nakamura et al. (1995, p. 331) also report that at the higher temperature the deformation of the rod was limited to the area adjacent to the defect. At the lower temperatures, the deformation was observed throughout the length of the rodlet. This may, however, be due in part to the marked difference in burnup for the higher temperature test. Also, at lower temperatures, the correspondingly lower rate of reaction with the oxygen will allow the oxygen to travel further along the rod before being consumed by oxidation.

6.2 SEMI-EMPIRICAL MODEL DEVELOPMENT

The data obtained from TGA tests on spent fuel fragments is used to develop a semi-empirical model for the incubation time, i.e., the time for an existing defect to start enlarging due to fuel dry-air oxidation, and clad splitting velocity at constant temperature. The analysis presented here is more comprehensive than presented in Hanson (1998) in that the effects of hydrated phases and grain sizes, in addition to burnup, are examined. However, the present model is not mechanistic. Neither grain size nor the mechanism of oxidation, i.e., diffusion through a product layer, is accounted for. These effects are present, however, in the recorded O/M as a function of time data. The present model can be used as a good estimate for clad degradation due to fuel oxidation for most CSNF, but smaller-grained fuels will react faster than those tested. The present model is limited in that it can not quantify these effects. The semi-empirical model is simply a fit to the data, and, as such, the use of the equivalent sphere model alleviates the importance of the parameters, such as grain size, for each grain. Hence, the derived equations are valid for a particle consisting of one large grain or, of many small grains of uniform size, assuming an ideal packing density. A mechanistic model such as that developed in Stout and Leider (1998) could be used to quantify grain size effects if necessary. TableCurve for Windows v1.11 by Jandel Scientific was used to perform the regressions on all of the data presented here (DTN: LL000402951021.133). Excel 97 was then used to vary the pre-exponential factors for the various cases chosen and to evaluate the equations with the given parameters. Hand calculations on random samples were performed to verify the software results.

It is assumed that all fuel is in contact with the cladding at time zero, i.e., there is no fuel/clad gap for any fuel upon emplacement. This assumption was made not only because it is the most conservative, but because there is no qualified expression that can be used to determine the fuel/clad gap for each fuel rod. It is known that the gap size is dependent on the initial gap, the time in reactor (burnup), and the temperature profile of both the fuel and cladding, with the gap closing over time in service due to swelling of the fuel pellets and creep of the cladding. The zero-gap assumption alleviates the need to determine the gap size for individual rods.

Once a waste package fails, oxygen is available to oxidize fuel in rods that have a pinhole or greater defect. No consideration for oxygen depletion or transport limitations was made. The fuel then oxidizes to $UO_{2.4}$, accompanied by a 0.7% volume reduction (see Table 3). The variations in $(O/M)_{\delta}$ have been ignored and it is assumed that the plateau occurs at an O/M ratio of 2.40. Further, it is assumed that conversion of an individual grain to $UO_{2.4}$ must be complete before oxidation to $UO_{2.75}$ begins. As seen in Table 1, the average time-rate-of-change in the

O/M ratio for the first 30 hours of oxidation is fairly uniform within a factor of three at a fixed temperature. The variations observed can, for the most part, be explained by variations in grain size, porosity, and cracking from sample to sample. The low-burnup samples, 105-15 through 105-18, however, exhibited faster rates of oxidation than other samples of higher burnup from the same fuel rod. This, and the lack of any observable plateau, may indicate that U_3O_8 formation was occurring simultaneously with the $UO_{2.4}$ phase.

Formation of $UO_{2.75}$ is accompanied by a volume expansion of 38% compared to the $UO_{2.4}$ phase. As the oxidation proceeds, the fuel grains expand until they again touch the clad. The reported strain needed for clad degradation varies from about 1% (Novak et al. 1983, p. 257) for a small crack to form, to about 2% (Novak et al. 1983, p. 263 and Nakamura et al. 1995, p. 331) for gross degradation in CANDU or BWR fuel, to 6.5% (Einziger and Cook 1985, p. 68) for crack propagation. For this analysis, it is assumed that zero strain is needed to initiate a crack at a defect. Thus, as soon as enough U_3O_8-like phase is formed for the fuel to touch the cladding, the incubation time has been reached. The analysis will also develop the equations to allow for a fuel/clad gap to exist upon emplacement and for some strain to be needed for crack initiation to occur.

6.3 DETERMINATION OF MODEL PARAMETERS FOR UO_2 TO $UO_{2.4}$ TRANSITION

6.3.1 Determining Extent of Reaction

The data for this analysis are listed in Table 1. The time to plateau, $t_{2.4}$, is, by definition of Hanson (1998), the time to reach $(O/M)_\delta$–0.005. To determine the actual time for complete conversion to $UO_{2.4}$, we must first be able to determine the extent of reaction of the individual grains. Figure 1 shows the volume of the fuel with respect to the clad at a given time. Note that this figure is illustrative only; it is not to scale.

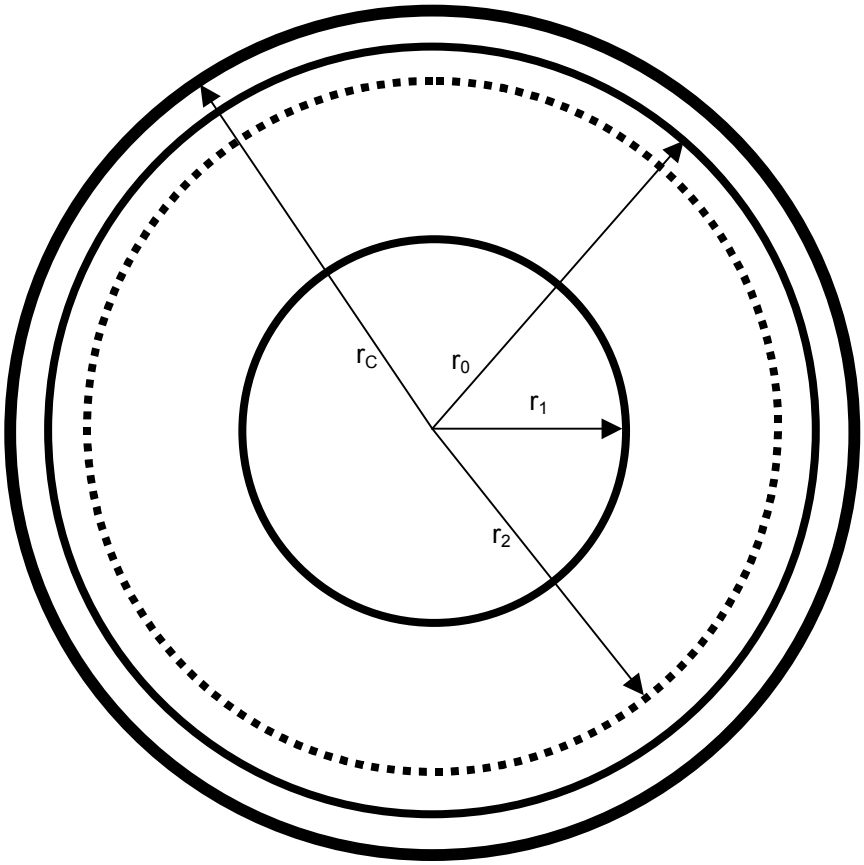

Figure 1. Relationship of Fuel to Clad for the UO_2 to $UO_{2.4}$ Transition

where,

r_C = inner radius of the cladding
r_0 = initial radius of the UO_2 pellet (r_0=r_C if there is no fuel/clad gap)
$r_1(t)$ = instantaneous radius of the remaining UO_2
$r_2(t)$ = instantaneous radius of remaining UO_2 + instantaneous radius of $UO_{2.4}$

If z_1 is defined as the volume of $UO_{2.4}$ formed per unit volume of UO_2 reacted, then the total volume of the fuel at any time $0 \le t \le t_{2.4}$ is (canceling the $4/3\pi$ in each term):

$$r_2^3 = z_1 r_0^3 + (1-z_1) r_1^3 \qquad \text{(Eq. 7)}$$

This equation assumes that the fuel and its grains can be approximated as spheres. For the purpose of this model, which again is semi-empirical and does not attempt to provide a detailed mechanistic interpretation of the oxidation process, the fuel pellet in the local region of concern can be approximated as a single spherical grain of initial radius r_0. Equation 7 is also valid as written if r is the half-grain length of a cubic grain (such as used in Stout and Leider 1998, Section 3.2.2) or if r is both the radius and height of a cylindrical grain. Note that if the fuel

consists of numerous grains, each assumed to be a uniform (i.e., same dimensions and properties, such as burnup) sphere (or cube or cylinder) with an ideal packing density, then Equation 7 still holds because each term is simply multiplied by N, the number of grains to occupy the same volume as the single grain. If the fuel consists of a distribution of grain sizes, as is actually observed, then this equation is still valid by summing over each individual population. Oxidation is a diffusion-controlled process, though, so smaller grains will react faster due to their relatively larger surface-to-volume ratio. This effect is accounted for in the present model only by fitting the O/M as a function of time data, which, in turn, is dependent on the grain size. The mechanistic model presented by Stout and Leider (1998, Section 3.2.2) explicitly accounts for grain size distributions and their effect on oxidation.

Since at completion of the $UO_{2.4}$ reaction there is no UO_2 remaining, it is clear that $r_1=0$ at $t=t_{2.4}$. Equation 7 then becomes

$$r_2^3 = z_1 r_0^3 \qquad (\text{at } t=t_{2.4}) \qquad \text{(Eq. 8)}$$

where, $z_1=0.9929$ from Table 3. Since Equation 7 has two unknowns, a second expression is needed to solve for r_2 (or the volume $4/3\pi r_2^3$), the radius of the fuel at any time t. A mass balance on the fuel gives

$$\text{mass } UO_{2.4}(t) + \text{mass } UO_2(t) = \text{initial mass } UO_2 + \Delta\text{mass} \qquad \text{(Eq. 9)}$$

where,

$$\Delta\text{mass} = \Delta(O/M)\times\text{initial mass } UO_2\times(16/270) \qquad \text{(Eq. 10)}$$

$\Delta(O/M)$ in turn is the change in the bulk O/M ratio from the initial O/M of 2.00 and is calculated as a function of time from the raw data (Δmass) of the TGA tests. As stated in Hanson (1998), this equation neglects any change in molecular weight of the spent fuel resulting from the addition of fission products and higher actinides. Recognizing that there will be a $4/3\pi$ term that can be canceled in each term in Equation 9 (the same is true for the factor N if multiple, uniform small grains are used), we have

$$(r_2^3-r_1^3)\rho_{2.4} + r_1^3\rho_{2.0} = r_0^3\rho_{2.0} + r_0^3\rho_{2.0}\Delta(O/M)(16/270) \qquad \text{(Eq. 11)}$$

where,

$\rho_{2.0}$ and $\rho_{2.4}$ are the densities of UO_2 and $UO_{2.4}$, respectively, as given in Table 3. Substituting Equation 7 into Equation 11 and solving for r_1/r_0 yields:

$$r_1/r_0 = [\ (\rho_{2.0} + \rho_{2.0}\,\Delta(O/M)\,(16/270) - z_1\,\rho_{2.4})/(\rho_{2.0} - z_1\,\rho_{2.4}\ )]^{1/3} \qquad \text{(Eq. 12)}$$

Since the actual fractional radius reacted, defined as the extent of reaction λ, is simply $(r_0-r_1)/r_0$, we can express the extent of reaction as

$$\lambda_{2.4} = 1 - r_1/r_0 \qquad \text{(Eq. 13)}$$

The time required to reach the plateau can be expressed in terms of the Arrhenius equation

$$t_{2.4} = k_{2.4} \exp(Q_{24}/RT) \quad \text{(Eq. 14)}$$

where,

$k_{2.4}$ is the pre-exponential factor for the UO_2 to $UO_{2.4}$ transition (h)
Q_{24} is the corresponding activation energy (J mol^{-1})
R is the universal gas constant (8.314 J mol^{-1} K^{-1})
and T is the temperature (K =273+T(°C)).

For a reaction to a Δ(O/M) in the range $2.0 \leq 2.0+\Delta(O/M) \leq 2.4$, equation 14 simply becomes

$$t_{\Delta(O/M)} = \lambda_{2.4}\, k_{2.4} \exp(Q_{24}/RT) \quad \text{(Eq. 15)}$$

Note that this expression is valid without knowledge of the reaction mechanism because it is simply an empirical fit to the data. To be mechanistic, the pre-exponential factor ($\lambda_{2.4}$ $k_{2.4}$) would have to reflect the diffusion through an reaction layer of increasing thickness and would be expressed in units such as μm^2 h^{-1}. This would fit an equation of the form

$$W = 2\,(kt)^{1/2} \quad \text{(Eq. 16)}$$

such as has been used in the Waste Form Characteristics Report (Stout and Leider 1998, Section 3.2.2), where W is the width of the oxidation front and k is the corresponding rate equation governing the mechanistic oxidation process. The grain size effect in the present analysis is not explicitly accounted for, but will appear in the Δ(O/M) as a function of time term in the equations above. However, since most samples were from the same section of a single fuel rod, the variations are expected to be small.

Table 1 includes data from TGA experiments where the O/M ratio as a function of time was monitored. The time to oxidize a sample from a bulk O/M ratio of 2.30 to 2.35 was measured, as was the time to oxidize from 2.0 to 2.395 (i.e., the definition of $t_{2.4}$.) To convert these times to the time it would take for full conversion to $UO_{2.4}$, use Equations 12 and 13 and normalize to obtain λ=1. For example, at a bulk O/M of 2.395 (Δ(O/M)=0.395), we calculate that r_1/r_0 is 0.232 and thus only 76.8% (1-0.232) of the grain has reacted. We now convert the time required to oxidize this fraction to the time to convert the entire grain by dividing by 0.768. This assumes that all grains in a multiple grain sample have equal access to oxygen and that there is no delay due to grain boundary oxidation or transport.

6.3.2 Temperature Dependence of the UO_2 to $UO_{2.4}$ Transition

The software program TableCurve for Windows by Jandel Scientific was used to fit the data from Table 1. Documentation of these fits is in Laboratory Record Book 57225 (DTN: LL000402951021.133). Figure 2 is a plot of the time required to oxidize a sample from a bulk O/M ratio of 2.30 to 2.35 as a function of temperature. All data were fitted using TableCurve (DTN: LL000402951021.133, pp. 38-42) to provide a nominal fit to data of the form ln(time) vs. 1/T. The slope of the straight-line fit is then Q/R, the activation energy divided by the

universal gas constant, while the exponent of the intercept is the pre-exponential factor. The activation energy Q_{24} was determined to be 123±17 kJ mol^{-1} (R^2=0.75). If the four low-burnup samples are ignored, mostly because of their smaller grain size and the possibility of forming U_3O_8 simultaneously with the $UO_{2.4}$, then the activation energy is 112±13 kJ mol^{-1} (R^2=0.84). Finally, if the low-burnup samples and the three samples known to have significant hydrated phases present, samples 105-01, 105-02, and 105-03, are ignored, then the activation energy is 107±13 kJ mol^{-1} (R^2=0.86).

This analysis was repeated (DTN: LL000402951021.133, pp. 48-52) for the time to reach the plateau, $t_{2.4}$. The nominal fit to the 18 ATM-105 data points and the 2 ATM-104 data points gives an activation energy of 137±29 kJ mol^{-1} (R^2=0.55). If the low burnup samples are removed from the analysis, the activation energy is 117±25 kJ mol^{-1} (R^2=0.60). The removal of these 4 samples is justified because it is likely that conversion to U_3O_8 was occurring simultaneously with the $UO_{2.4}$ transition. This would explain the faster initial rates of oxidation for these samples, the lower $(O/M)_\delta$, and the lack of any real plateau. If only the 9 data points of ATM-105 fuel of similar burnup and grain size, without identifiable hydrated phases present, and with no data collection problems are fitted, the activation energy obtained is 123±18 kJ mol^{-1} (R^2=0.87). Figure 3 is a plot of the time to plateau as a function of temperature with two of these three fits included for comparison. Clearly, at lower activation energies the time to convert the UO_2 to $UO_{2.4}$ is smaller at the lower temperatures of interest to the repository.

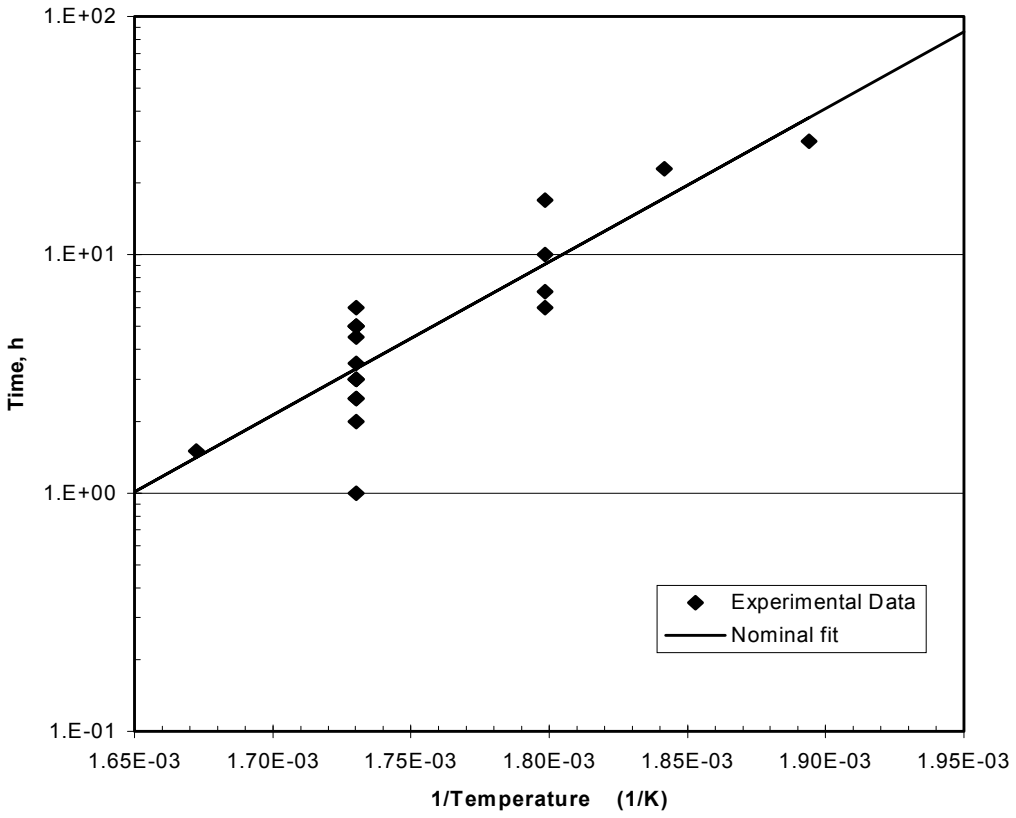

Figure 2. Time to Oxidize CSNF Fragments from $UO_{2.30}$ to $UO_{2.35}$ as a Function of Temperature

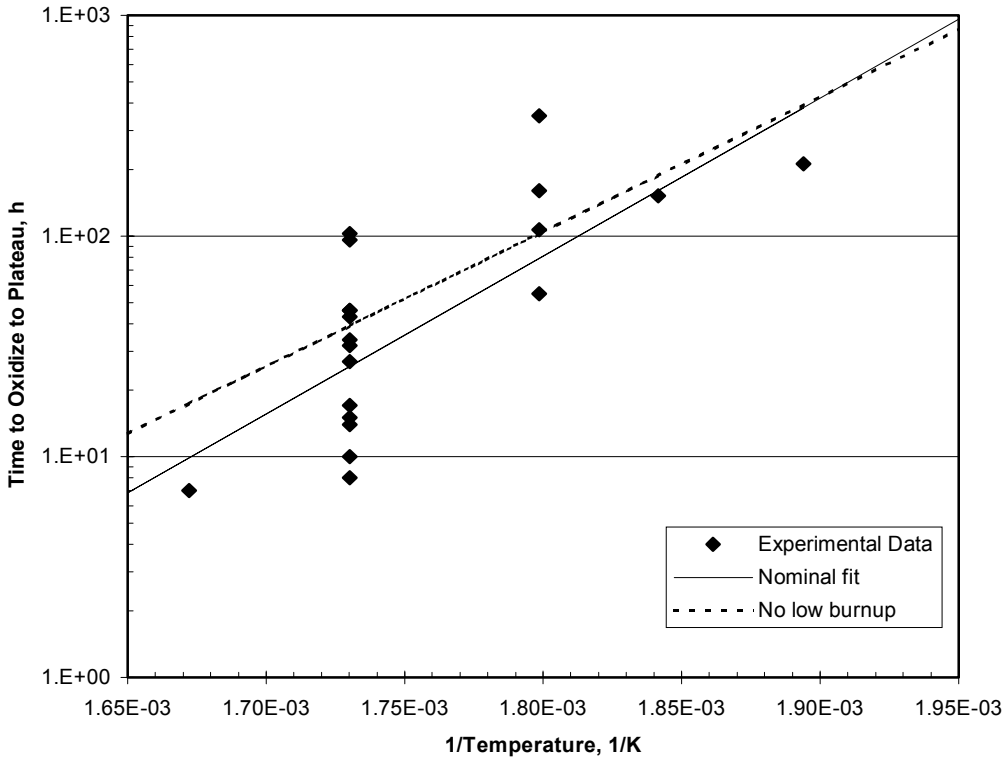

Figure 3. Time to Oxidize CSNF Fragments to the Plateau as a Function of Temperature

Woodley et al. (1989, p. 84) reported an activation energy of 113±17 kJ mol^{-1} for Turkey Point fuel oxidized in the same TGA systems. McEachern and Taylor (1998, p. 110) performed an extensive review of literature data and determined that for spent fuel, the best estimate for the activation energy of the UO_2 to $UO_{2.4}$ conversion is ~106 kJ mol^{-1}. The best fit to the $UO_{2.30} \rightarrow UO_{2.35}$ transition was 107 kJ mol^{-1}, and if we subtract one standard deviation from the best fit for the time to plateau data, the activation energy is 105 kJ mol^{-1}. Thus, to provide the best estimate for the time to complete the conversion to $UO_{2.4}$ and to maintain conservatism at the lower temperatures, an activation energy for this first transition was chosen as 105 kJ mol^{-1}.

The analyses above were repeated, but the data was fitted to a straight line equation where the slope was fixed to correspond to the activation energy of 105 kJ mol^{-1}. Nominal fits to the data were obtained and the pre-exponential factor was found by taking the exponent of the intercept. By definition, the nominal fit is such that some data points had faster times of oxidation than predicted by the resulting equation. The nominal fit chosen for the analysis was the fit to the data where the low-burnup, smaller-grained samples and those samples known to have hydrated phases present were removed from the analysis. The nominal fit is representative of moderate and higher burnup samples without hydrated phases. The pre-exponential factor was adjusted, keeping the activation energy fixed, so that the model was conservative for all data points being considered. The fit obtained by this method is considered the bounding case and is valid for all of the fuels tested. The data point that controls the bounding case fit is sample 105-18, a low-

burnup, smaller-grained sample that had the presence of a hydrated phase confirmed using X-ray diffractometry (DTN: LL000314651021.132).

However, it must be stressed that fuels with even smaller grains may oxidize faster than predicted by these parameters. Samples with larger quantities of hydrated phases present may also oxidize faster than the bounding case fits. Figures 4 and 5 plot the data with the nominal and bounding case fits using the activation energy of 105 kJ mol^{-1}. Table 7 identifies the value of the pre-exponential factor for each of the cases.

Table 7. Nominal and Bounding Case Fits for the UO_2 to $UO_{2.4}$ Transition

	Nominal Case		Bounding Case	
	$UO_{2.30}$ to $UO_{2.35}$	$t_{2.4}$	$UO_{2.30}$ to $UO_{2.35}$	$t_{2.4}$
k (h)	1.411×10^{-9}	1.318×10^{-8}	3.241×10^{-10}	2.592×10^{-9}

From Section 6.3.1, we find that the extent of conversion for the $UO_{2.30}$ to $UO_{2.35}$ transition is equivalent to only 13% of the radius; thus we divide k by 0.13 to obtain $k_{2.4}$, which represents the factor for full conversion to $UO_{2.4}$. Similarly, the extent of conversion for the time to plateau, $t_{2.4}$, as defined in Hanson (1998) is 76.8%. Thus to obtain $k_{2.4}$ from k for $t_{2.4}$, we divide k by 0.768. The two values for k for the nominal case were divided by the appropriate normalization constants to obtain $k_{2.4}$. The two values of $k_{2.4}$ were then averaged to obtain the nominal value of the pre-exponential $k_{2.4}$ as listed in Table 8. This normalization and averaging was repeated for the bounding case. Note that the bounding case is almost a factor of 5 faster than the nominal case, apparently due to the presence of hydrated phases prior to oxidation. This factor is in excellent agreement with observations reported in Sections 6.1.5.2 and 6.1.6.2.

Table 8. Nominal and Bounding Case Values for $k_{2.4}$

	Nominal Case	Bounding Case
$k_{2.4}$ (h)	1.40×10^{-8}	2.93×10^{-9}

The time to plateau, now also called $t_{2.4}$ but representing full conversion of the grains to $UO_{2.4}$, can be calculated for any temperature using Equation 14 with values of $k_{2.4}$ taken from Table 8 and Q_{24}=105 kJ mol^{-1}. The time to obtain any O/M in the range 2.0 to 2.4 can be obtained using these values in Equation 15 and calculating λ using Equations 12 and 13. For the purposes of this analysis, only the time for full conversion is important since no clad degradation occurs for this transition. However, it is important to note that fission gases and other volatile species that are located on the grain boundaries and possibly even in the fuel matrix may be released during this initial oxidation period. Table 9 lists the time to plateau for a variety of temperatures for both cases (assume 1 yr =8766 h).

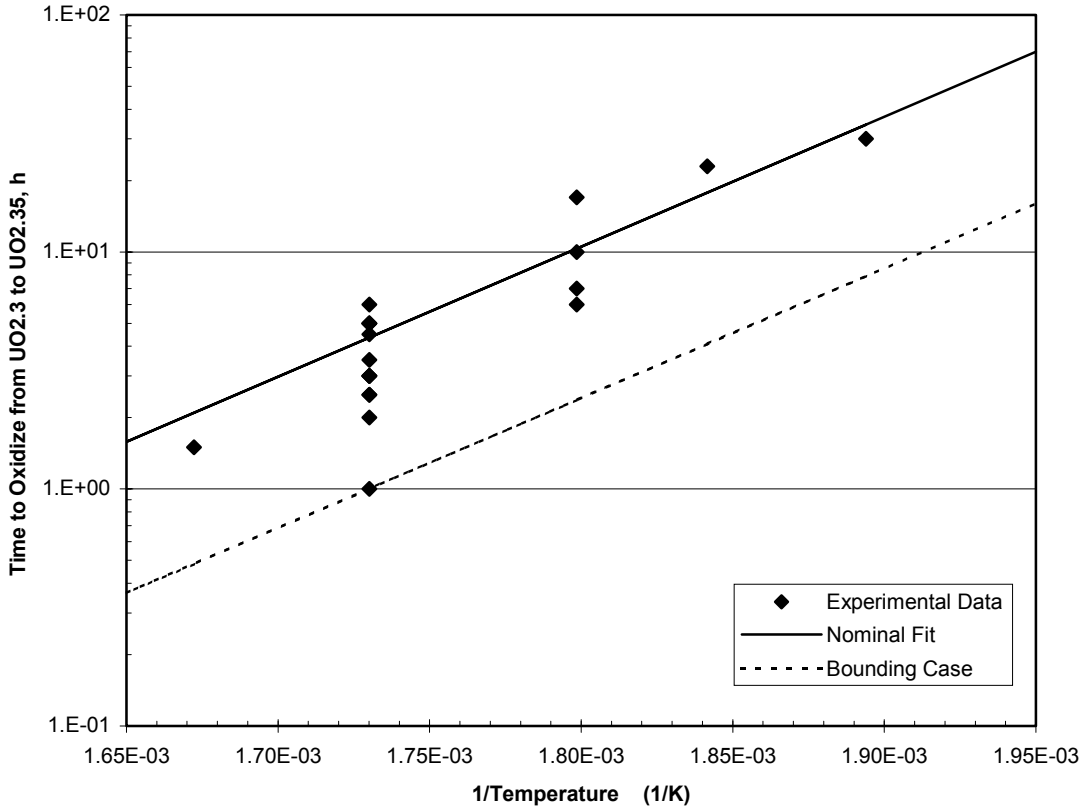

Figure 4. Nominal and Bounding Case Fits to $UO_{2.30}$ to $UO_{2.35}$ Data

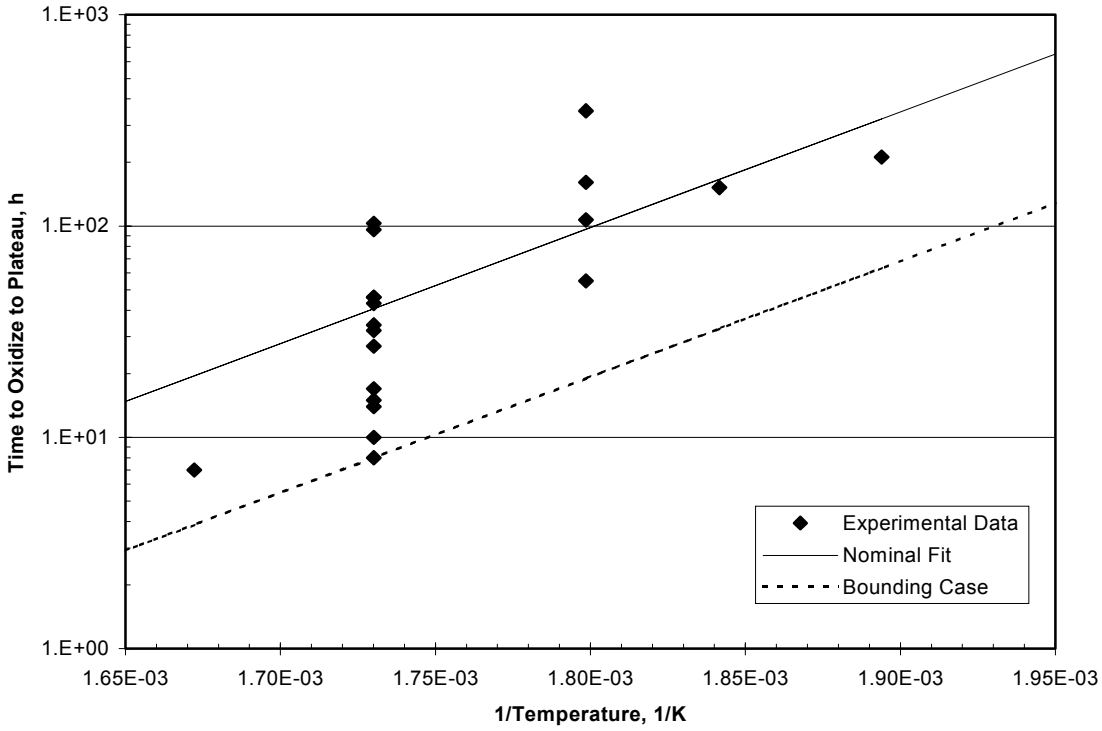

Figure 5. Nominal and Bounding Case Fits to Time to the Plateau Data

Table 9. Time for Complete Conversion to $UO_{2.4}$ as a Function of Temperature

Temperature (°C)	Nominal Case		Bounding Case	
	h	yr	h	yr
75	8.08×10^{7}	9.21×10^{3}	1.69×10^{7}	1.93×10^{3}
100	7.09×10^{6}	8.09×10^{2}	1.48×10^{6}	1.69×10^{2}
125	8.45×10^{5}	9.65×10^{1}	1.77×10^{5}	2.02×10^{1}
150	1.30×10^{5}	1.48×10^{1}	2.71×10^{4}	3.09×10^{0}
175	2.45×10^{4}	2.79×10^{0}	5126	5.85×10^{-1}
195	7343	8.38×10^{-1}	1537	1.75×10^{-1}
200	5520	6.30×10^{-1}	1155	1.32×10^{-1}
225	1445	1.65×10^{-1}	302	3.45×10^{-2}
250	430	4.90×10^{-2}	90	1.03×10^{-2}
275	143	1.63×10^{-2}	30	3.41×10^{-3}
283	103	1.17×10^{-2}	21	2.45×10^{-3}
300	52	5.96×10^{-3}	11	1.25×10^{-3}
305	43	4.93×10^{-3}	9	1.03×10^{-3}
325	21	2.37×10^{-3}	4	4.97×10^{-4}

The model developed for the oxidation transition of UO_2 to $UO_{2.4}$ was partially validated by comparison of both the model parameters (such as the activation energy discussed previously) and the model output (See Table 9) with values obtained from open literature. The dry-bath data reported in Hanson (1998, Section 4.3) show that for similar fuels, the time to plateau is about 3×10^4 hours at 175°C, about 10^4 hours at 195°C, and about 400 hours at 255°C. The nominal case matches these values fairly well and the bounding case is definitely conservative. The times estimated here also agree fairly well, with the original equation of Einziger et al. (1992, Equation 3, p. 59)

$$t_{2.4}(h) = 2.6\times10^{-9} \exp(111 \text{ kJ mol}^{-1}/RT) \qquad \text{(Eq. 17)}$$

which was obtained using the 175°C and 195°C dry-bath data and values at lower temperatures from EPRI (1986). Because of the smaller activation energy used in the present model, the nominal times to reach the plateau as predicted by the model will be conservative when compared with the equation of Einziger et al. (1992) at the temperatures of interest in the repository, i.e., ≤150°C. Confirmatory data from additional oxidation tests will be used to further validate the model.

6.4 DETERMINATION OF MODEL PARAMETERS FOR $UO_{2.4}$ TO $UO_{2.75}$ TRANSITION

6.4.1 Burnup Dependence of the $UO_{2.4}$ to $UO_{2.75}$ Transition

The data in Table 2 were analyzed, following the methodology in Hanson (1998), to determine the burnup dependence of the $UO_{2.4}$ to $UO_{2.75}$ transition. It was hypothesized that the soluble fission products and higher actinides stabilize the cubic matrix and make it more difficult for the matrix to transition to the orthorhombic structure of $UO_{2.75}$ (hyperstoichiometric phase of U_3O_8). This being the case, a simple linear dependence of the activation energy on burnup was proposed, as represented by Equation 18.

$$Q_{75} = Q_{75}^{0} + \alpha \times B \qquad \text{(Eq. 18)}$$

where Q_{75} is the total activation energy for the $UO_{2.4}$ to $UO_{2.75}$ transition (kJ mol^{-1})
Q_{75}^{0} is the Arrhenius activation energy for the $UO_{2.4}$ to $UO_{2.75}$ transition (kJ mol^{-1})
α is the burnup dependent constant for the activation energy (kJ mol^{-1} per MWd/kg M)
B is the burnup of the sample (MWd/kg M)

A plot of the logarithm of time as a function of burnup (for samples oxidized at a fixed temperature) yields a slope equal to α/RT. For the purposes of this analysis, this methodology is more than adequate. However, burnup alone does not necessarily fully describe the true dependence on total soluble impurity concentration. This is a function of the isotope fissioned and, therefore, of enrichment and of the temperature distribution of the fuel that is related to thermal conductivity (a function of burnup and porosity) and the linear heat generation rate.

As documented in DTN: LL000402951021.133 (pp. 17-19, 25-26), there are three different data sets used to calculate the burnup dependent constant. Using the data set for duration of the plateau at 305°C, α=1.4±0.2 kJ mol^{-1} per MWd/kg M (R^2=0.88). The plateau behavior is strongly influenced by the grain size and is skewed by the low-burnup samples that may have been forming $UO_{2.75}$ concurrently with the $UO_{2.4}$. When these samples were removed from the analysis, a value α=1.0±0.3 kJ mol^{-1} per MWd/kg M (R^2=0.69) was obtained. If samples with known hydrated phases are removed as well, then α=0.9±0.2 kJ mol^{-1} per MWd/kg M (R^2=0.81). When the entire data set for the time to oxidize from $UO_{2.45}$ to $UO_{2.50}$ at 305°C was used, then α=1.1±0.1 kJ mol^{-1} per MWd/kg M (R^2=0.86). The data set is too limited to repeat the analysis with the low burnup and hydrated samples removed and still have a meaningful fit. Finally, the entire data set for the time to oxidize from $UO_{2.54}$ to $UO_{2.59}$ at 305°C was used, and a value of α=1.1±0.3 kJ mol^{-1} per MWd/kg M (R^2=0.70) was obtained. These values correspond to the previous analysis of this data set (Hanson 1998). For a fixed value of the Arrhenius activation energy, a smaller value of α would be conservative. Thus, a nominal value of α=1.0 kJ mol^{-1} per MWd/kg M was chosen and is used in calculating the activation energy of the $UO_{2.4}$ to $UO_{2.75}$ transition.

6.4.2 Temperature Dependence of the $UO_{2.4}$ to $UO_{2.75}$ Transition

Plots of the natural logarithm of the time on plateau as a function of inverse temperature with a straight line were plotted. The slope is equal to Q_{75}/R. Using the average value of the burnups of the samples being fitted and α=1.0 kJ mol^{-1} per MWd/kg M, the Arrhenius activation energy Q_{75}^{0} can be calculated from Equation 18 (DTN: LL000402951021.133, pp. 58-60). When all data points are used for the analysis, we obtain Q_{75}=367±111 kJ mol^{-1} (R^2=0.39) and with an average burnup of 28 MWd/kg M the value of Q_{75}^{0} is 339 kJ mol^{-1}. Remember that the time on plateau, as defined for this analysis, includes the time to complete the oxidation to $UO_{2.4}$ of the final ~24% of the initial grain radius. This duration of the plateau is thus highly grain size dependent and will also be affected by the presence of hydrated phases accelerating the transition to $UO_{2.75}$. When the data set is narrowed to include only specimens of ATM-105 fuel of moderate burnup and similar grain size and without confirmed hydrated phases, Q_{75}=236±27 kJ mol^{-1} (R^2=0.91) is obtained. Again, with an average burnup of 28 MWd/kg M, the value of Q_{75}^{0}

is 208 kJ mol^{-1} and can be as small as 181 kJ mol^{-1} if the one standard deviation uncertainty is subtracted.

This analysis was repeated (DTN: LL000402951021.133, pp. 61-63) using the data for the time to oxidize from $UO_{2.45}$ to $UO_{2.50}$ or times just shortly after the plateau. Note (see Table 2) that most of the higher burnup samples and samples oxidized at lower temperatures did not oxidize long enough for these levels of oxidation to be achieved. Still, when all available data points are used, the total activation energy is calculated as 217±89 kJ mol^{-1} (R^2=0.31). The corresponding value for the Arrhenius activation energy is 189 kJ mol^{-1}. When the low burnup and hydrated samples are ignored, as well as the higher burnup 104-01 sample, we obtain Q_{75}=147±19 kJ mol^{-1} (R^2=0.92) and Q_{75}^0 is 119 kJ mol^{-1}. It must be noted that there are only seven data points covering three temperatures in this final analysis with only one data point at each of two temperatures.

The final analysis (DTN: LL000402951021.133, pp. 64-66) to determine the activation energies was performed on the data for the time to oxidize from $UO_{2.54}$ to $UO_{2.59}$. Note from Table 2 that there are even fewer data points available for this analysis. The nominal fit to all data points gives Q_{75}=225±71 kJ mol^{-1} (R^2=0.48) and with an average burnup of 25 MWd/kg M the value of Q_{75}^0 is 200 kJ mol^{-1}. Again ignoring the low burnup samples or those with hydrated phases present, Q_{75}=148±24 kJ mol^{-1} (R^2=0.88) and Q_{75}^0 is about 120 kJ mol^{-1}.

McEachern et al. (1997, Equation 37, p. 66) and McEachern and Taylor (1998, p. 113) performed a detailed analysis to determine the activation energy for the formation of U_3O_8 on UO_2 and reported values for Q_{75}^0 as 146±10 kJ mol^{-1} and 154 kJ mol^{-1}, respectively. While the Arrhenius activation energy for unirradiated fuel is not necessarily the same as for spent fuel, within the rather large uncertainties of our limited data set, our values of Q_{75}^0 agree fairly well with those reported in literature. The exception is the time on plateau, which consistently has higher activation energies than those calculated by the other means. One very probable explanation is that the plateau is also a result of the higher activation energy needed to nucleate U_3O_8 sites on the $UO_{2.4}$ phase. Once these sites are present in sufficient number, the $UO_{2.75}$ grows fairly uniformly. If this is true, then as seen here, it is likely that the additional activation energy required to nucleate sites is on the order of 30 kJ mol^{-1} higher. However, there is not enough data to support this hypothesis at this time, so this mechanism is not included in this analysis. Any plateau formation is due solely to the observation that no U_3O_8 forms until conversion to $UO_{2.4}$ is complete, a grain size distribution with large grains requiring longer to convert to $UO_{2.4}$, and the higher activation energy to form $UO_{2.75}$. Neglect of any explicit plateau behavior is conservative. Given the large uncertainties due to the limited data set, and especially the small range of temperatures tested, an average of the literature values yields Q_{75}^0 = 150 kJ mol^{-1}. This value is conservative when compared to the fits from the duration of the plateau data and conservative for the values obtained for the other two data sets when all available data points were used.

TableCurve was then used to again fit the data to derive the pre-exponential factor for the nominal case (DTN: LL000402951021.133, pp. 67, 69). The slope of the straight-line fit to a plot of the natural logarithm of the time as a function of inverse temperature was fixed at Q_{75};

with Q_{75}^0 being 150 kJ mol^{-1}, α being 1.0 kJ mol^{-1} per MWD/kg M, and the burnup being the average of all data points being fitted. The nominal fit was chosen as the case to fit the moderate burnup ATM-105 samples that did not display evidence of hydrated phases. Excel was used to vary the pre-exponential factor until all data was above the model prediction, thus being conservative (DTN: LL000402951021.133, pp. 68,70). Again, the bounding case is that value of the pre-exponential needed to fit the 105-18 data point, which is a low-burnup, smaller-grained sample with hydrated phases present. Figures 6 and 7 plot the data with the nominal and bounding case fits for the $UO_{2.45}$ to $UO_{2.50}$ and $UO_{2.54}$ to $UO_{2.59}$ transitions, respectively. The duration of the plateau was not analyzed because of the potential problems resulting from how it was calculated, as discussed above. The times to complete oxidation to $UO_{2.75}$ was not used because of the limited data set that is biased toward the low burnup and hydrated phase samples.

The pre-exponential factors needed to fit an equation of the form

$$t(h) = k(h) \exp((Q_{75}^0 + \alpha \times \text{Burnup})/RT) \qquad \text{(Eq. 19)}$$

are given in Table 10.

Table 10. Nominal and Bounding Case Fits for the $UO_{2.4}$ to $UO_{2.75}$ Transition

	Nominal Case		Bounding Case	
	$UO_{2.45}$ to $UO_{2.50}$	$UO_{2.54}$ to $UO_{2.59}$	$UO_{2.45}$ to $UO_{2.50}$	$UO_{2.54}$ to $UO_{2.59}$
k (h)	2.816×10^{-15}	3.400×10^{-15}	1.011×10^{-15}	8.420×10^{-16}

These values must be corrected for the extent of conversion, discussed in the next section, to be used uniformly for the $UO_{2.4}$ to $UO_{2.75}$ transition.

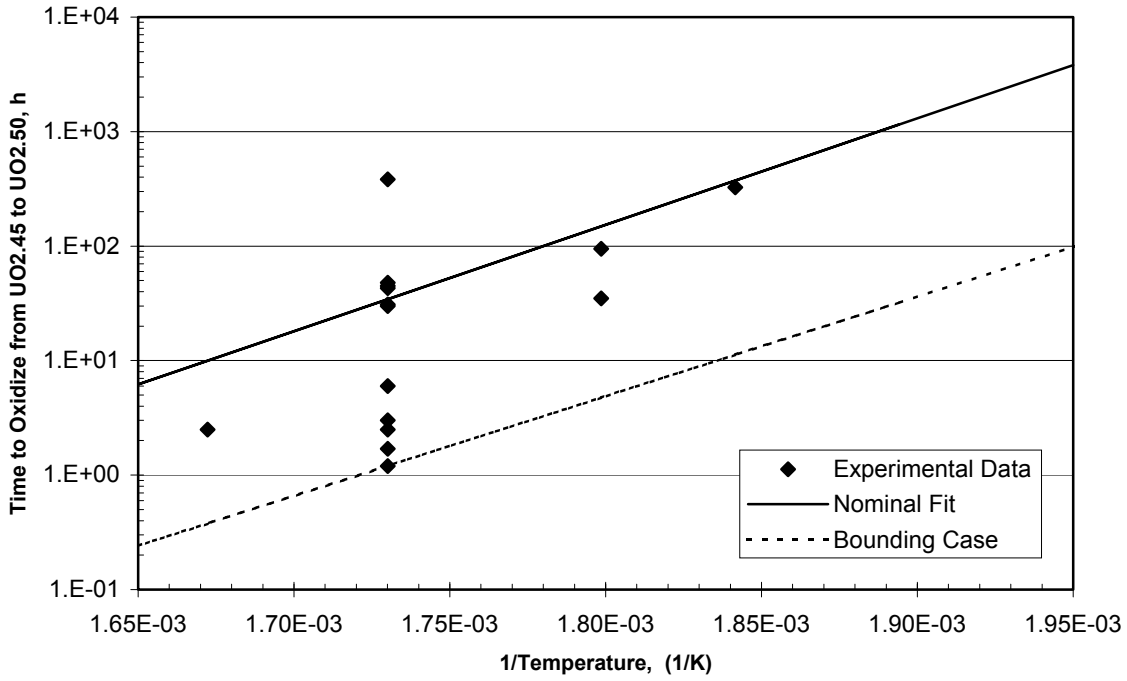

Figure 6. Nominal and Bounding Case Fits to $UO_{2.45}$ to $UO_{2.50}$ Data

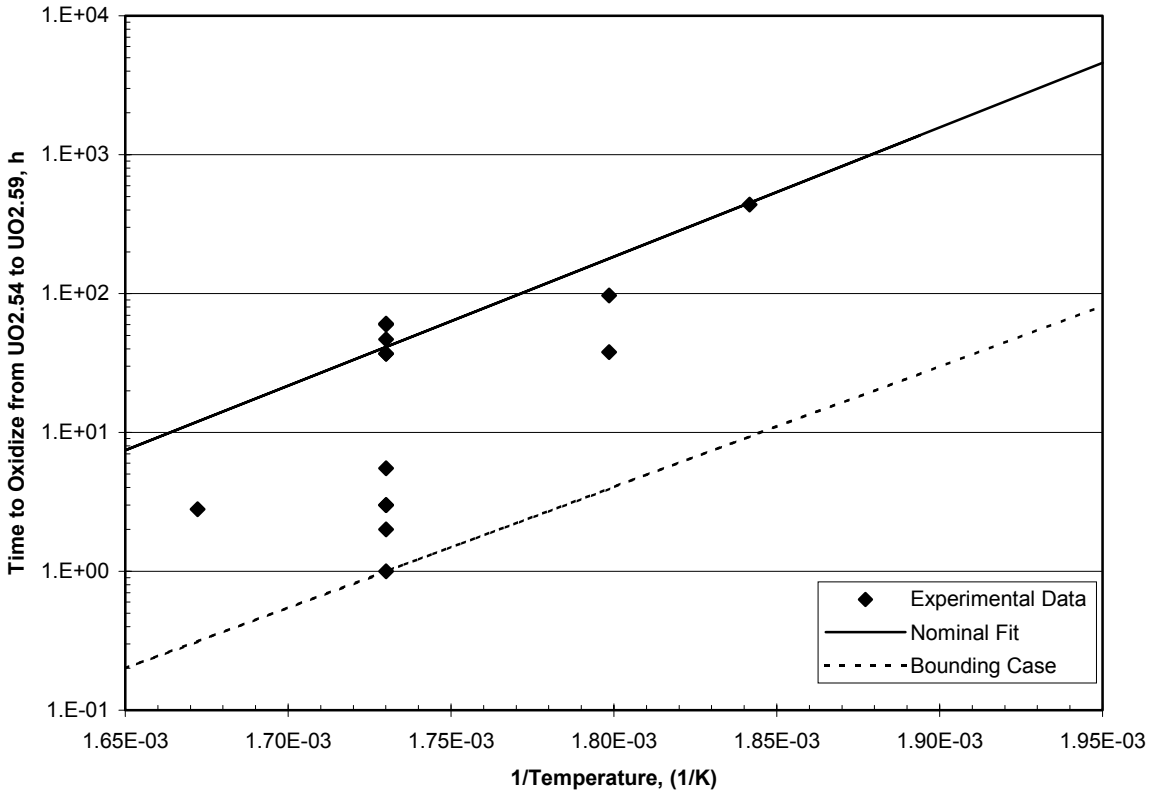

Figure 7. Nominal and Bounding Case Fits to $UO_{2.54}$ to $UO_{2.59}$ Data

6.4.3 Determining Extent of Reaction for the $UO_{2.4}$ to $UO_{2.75}$ Transition

Figure 8 illustrates the individual volumes of the fuel with respect to the clad for times $t_{2.4} \le t \le t_{inc}$ where t_{inc} is the incubation time needed to initiate crack growth. For this analysis, where zero stress is assumed, at t_{inc} we have the condition that $r_{21}=r_C$, which is also equal to r_0 for the zero initial fuel/clad gap assumption. For times greater than t_{inc}, then $r_{21}>r_C$ and continues to grow until conversion is complete.

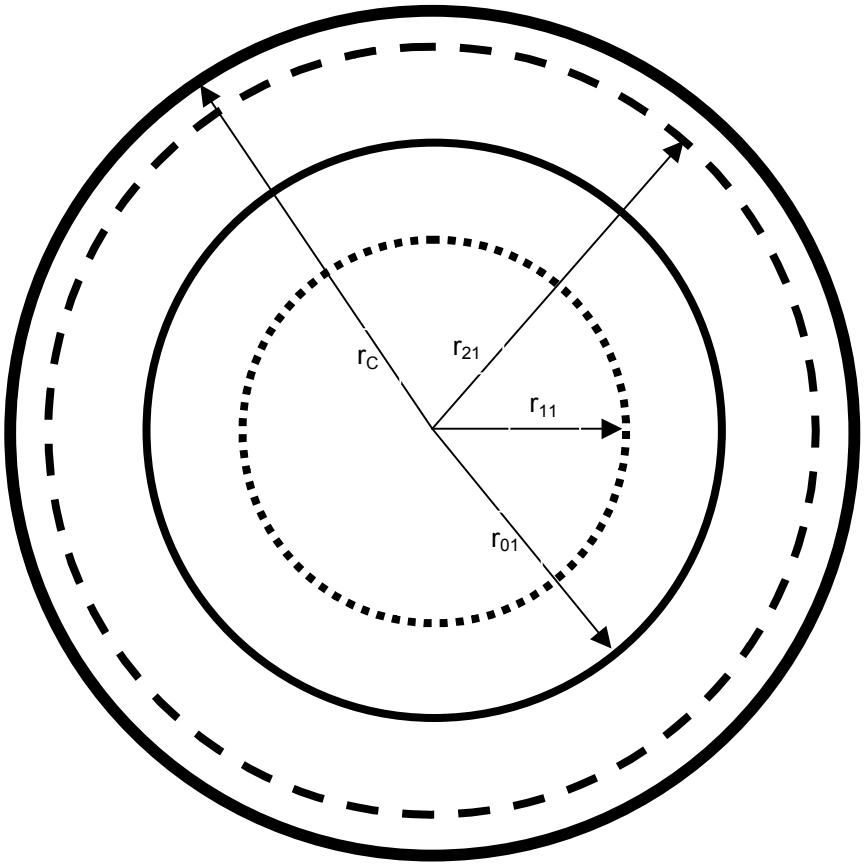

Figure 8. Relationship of Fuel to Clad for the $UO_{2.4}$ to $UO_{2.75}$ Transition

where

r_C = inner radius of the cladding
r_{01} = initial radius of the $UO_{2.4}$ pellet ($r_{01} = r_2$ at full conversion to $UO_{2.4}$)
$r_{11}(t)$ = instantaneous radius of remaining $UO_{2.4}$
$r_{21}(t)$ = instantaneous radius of remaining $UO_{2.4}$ + instantaneous radius of $UO_{2.75}$

We now define z_2 as the volume of $UO_{2.75}$ formed per unit volume of $UO_{2.4}$ reacted. From Table 3 we find that $z_2=1.3807$. Then for any time $t_{2.4} \le t \le t_{2.75}$ we again have an expression of the form

$$r_{21}^3 = z_2\, r_{01}^3 + (1-z_2)\, r_{11}^3 \qquad \text{(Eq. 20)}$$

Again, it is assumed that the fuel in the local region of interest may be approximated as a single spherical grain. This model is only a fit to the data and does not purport to model the actual oxidation mechanism. As such, the single grain assumption is as valid as a multi-grain one and is, in fact, equivalent if a uniform packing density is assumed. The equations and derivations remain the same for a cubic grain of half-grain dimension r or for a cylindrical grain of radius and height r. Using the same methodology as for Equations 8 though 12, we can solve for r_{11}/r_{01} and find

$$r_{11}/r_{01} = [\ (\rho_{2.4} + (\rho_{2.0}/z_1)\ \Delta(O/M)\ (16/270) - z_2\ \rho_{2.75})/(\rho_{2.4} - z_2\ \rho_{2.75}\ )]^{1/3} \qquad \text{(Eq. 21)}$$

remembering that since the conversion to $UO_{2.4}$ is complete prior to any formation of $UO_{2.75}$, $r_{01} = (z_1)^{1/3}\ r_0$. Note that because the cube root is taken, truncation and the number of significant digits used in the calculations can affect the values calculated. Simplifying the expression above gives

$$r_{11}/r_{01} = [\ 1 + (((\rho_{2.0}/z_1)\ \Delta(O/M)\ (16/270))/(\rho_{2.4} - z_2\ \rho_{2.75}\ ))]^{1/3} \qquad \text{(Eq. 22)}$$

The extent of reaction for this transition is then

$$\lambda_{75} = 1 - r_{11}/r_{01} \qquad \text{(Eq. 23)}$$

The time required to oxidize a sample from $UO_{2.4}$ to $UO_{2.75}$ is then simply

$$t_{2.75} = k_{75}\ \exp(Q_{75}/RT) \qquad \text{(Eq. 24)}$$

For a reaction $\Delta(O/M)$ in the range $2.4 \le 2.4+\Delta(O/M) \le 2.75$, the time required to oxidize to the bulk O/M ratio $2.4+\Delta(O/M)$ from the starting O/M of 2.4 is

$$t_{\Delta(O/M)75} = \lambda_{75}\ k_{75}\ \exp(Q_{75}/RT) \qquad \text{(Eq. 25)}$$

Using Equations 22 and 23, we find that for the transition from $UO_{2.45}$ to $UO_{2.50}$, only 5.6% of the radius r_{01} reacted. Thus, to get k_{75}, we divide the k for this fit by 0.0560. Similarly, for the $UO_{2.54}$ to $UO_{2.59}$ transition, 7.31% reacted. Normalizing the values in Table 10 as discussed in Section 6.3.2 and averaging for the two cases, we obtain the final values of k_{75} to use for this analysis, as listed in Table 11.

Table 11. Nominal and Bounding Case Values for k_{75}

	Nominal Case	Bounding Case
k_{75} (h)	4.84×10^{-14}	1.48×10^{-14}

Again, we see that the pre-exponential factor for the bounding case is a factor of about 3 smaller than the nominal case. Equivalently, for the bounding case, the time for oxidation from $UO_{2.4}$ to $UO_{2.75}$ is about three times faster than for the nominal case. Table 12 lists some typical times required to oxidize a sample from $UO_{2.4}$ to $UO_{2.75}$ as a function of temperature and burnup (Eq. 18 and Eq. 24) for the nominal case. It was assumed that 1 year equals 8766 hours (24*365.25). Table 13 lists the times for oxidation using the pre-exponential factor for the bounding case.

Data from Table 2 for the few samples that were oxidized to completion are compared with the predicted values from Equation 24 in Table 14. The data are actually the time from the plateau, $(O/M)_8$+0.005, to $UO_{2.75}$. Within the relatively large uncertainties resulting from the uncertainty in burnups of 1 to 2 MWd/kg M, the agreement is quite good. It is also clear that the rapid oxidation of samples 105-01, 105-02, 105-03, and 105-18 is accounted for by the bounding case, which considers the presence of hydrated phases.

Table 12. Time (yr) for Complete Conversion from $UO_{2.4}$ to $UO_{2.75}$ as a Function of Temperature and Burnup- Nominal Case

Temperature	Burnup (MWd/kg M)					
(°C)	0	10	20	30	40	50
75	1.81×10^{5}	5.47×10^{6}	1.82×10^{8}	5.77×10^{9}	1.83×10^{11}	5.79×10^{12}
100	5.61×10^{3}	1.41×10^{5}	3.54×10^{6}	8.91×10^{7}	2.24×10^{9}	5.64×10^{10}
125	2.69×10^{2}	5.52×10^{3}	1.13×10^{5}	2.33×10^{6}	4.78×10^{7}	9.81×10^{8}
150	1.84×10^{1}	3.17×10^{2}	5.44×10^{3}	9.34×10^{4}	1.60×10^{6}	2.76×10^{7}
175	1.71×10^{0}	2.50×10^{1}	3.66×10^{2}	5.37×10^{3}	7.87×10^{4}	1.15×10^{6}
195	3.05×10^{-1}	3.99×10^{0}	5.21×10^{1}	6.81×10^{2}	8.90×10^{3}	1.16×10^{5}
200	2.03×10^{-1}	2.58×10^{0}	3.28×10^{1}	4.17×10^{2}	5.31×10^{3}	6.75×10^{4}
225	2.99×10^{-2}	3.35×10^{-1}	3.75×10^{0}	4.19×10^{1}	4.70×10^{2}	5.25×10^{3}
250	5.29×10^{-3}	5.28×10^{-2}	5.27×10^{-1}	5.25×10^{0}	5.24×10^{1}	5.22×10^{2}
275	1.10×10^{-3}	9.85×10^{-3}	8.85×10^{-2}	7.94×10^{-1}	7.13×10^{0}	6.40×10^{1}
283	6.83×10^{-4}	5.94×10^{-3}	5.17×10^{-2}	4.50×10^{-1}	3.91×10^{0}	3.41×10^{1}
300	2.61×10^{-4}	2.13×10^{-3}	1.74×10^{-2}	1.42×10^{-1}	1.16×10^{0}	9.43×10^{0}
305	1.99×10^{-4}	1.59×10^{-3}	1.28×10^{-2}	1.02×10^{-1}	8.19×10^{-1}	6.56×10^{0}

Table 13. Time (yr) for Complete Conversion from $UO_{2.4}$ to $UO_{2.75}$ as a Function of Temperature and Burnup- Bounding Case

Temperature	Burnup (MWd/kg M)					
(°C)	0	10	20	30	40	50
75	5.54×10^{4}	1.75×10^{6}	5.56×10^{7}	1.76×10^{9}	5.59×10^{10}	1.77×10^{12}
100	1.71×10^{3}	4.31×10^{4}	1.08×10^{6}	2.73×10^{7}	6.85×10^{8}	1.72×10^{10}
125	8.21×10^{1}	1.69×10^{3}	3.46×10^{4}	7.11×10^{5}	1.46×10^{7}	3.00×10^{8}
150	5.64×10^{0}	9.68×10^{1}	1.66×10^{3}	2.86×10^{4}	4.91×10^{5}	8.43×10^{6}
175	5.22×10^{-1}	7.64×10^{0}	1.12×10^{2}	1.64×10^{3}	2.41×10^{4}	3.53×10^{5}
195	9.33×10^{-2}	1.22×10^{0}	1.59×10^{1}	2.08×10^{2}	2.72×10^{3}	3.55×10^{4}
200	6.21×10^{-2}	7.89×10^{-1}	1.00×10^{1}	1.28×10^{2}	1.62×10^{3}	2.06×10^{4}
225	9.15×10^{-3}	1.02×10^{-1}	1.15×10^{0}	1.28×10^{1}	1.44×10^{2}	1.61×10^{3}
250	1.62×10^{-3}	1.61×10^{-2}	1.61×10^{-1}	1.61×10^{0}	1.60×10^{1}	1.60×10^{2}
275	3.36×10^{-4}	3.01×10^{-3}	2.71×10^{-2}	2.43×10^{-1}	2.18×10^{0}	1.96×10^{1}
283	2.09×10^{-4}	1.82×10^{-3}	1.58×10^{-2}	1.38×10^{-1}	1.20×10^{0}	1.04×10^{1}
300	7.98×10^{-5}	6.51×10^{-4}	5.31×10^{-3}	4.33×10^{-2}	3.54×10^{-1}	2.88×10^{0}
305	6.08×10^{-5}	4.87×10^{-4}	3.90×10^{-3}	3.13×10^{-2}	2.50×10^{-1}	2.01×10^{0}

Table 14. Comparison of Actual Times (from Table 2) for Complete Conversion of $UO_{2.4}$ to $UO_{2.75}$ with Model

Sample Identification	Estimated Time-Nominal Case (h)	Estimated Time-Bounding Case (h)	Actual Time (h)
105-01[a]	2559	782	585
105-01[b]	1660	508	585
105-02[a]	171	52	78
105-03	603	184	112
105-11	382	117	674
105-11[c]	824	252	674
105-12	579	177	585
105-13	629	192	611
105-14	603	184	513
105-15	93	28	64
105-16	78	24	89
105-17	56	17	21
105-18	57	17	16

NOTES: [a] Estimated burnup of 28 MWd/kg M.
[b] Estimated burnup of 26 MWd/kg M.
[c] Using burnup of 29.6 MWd/kh M from Nd-analysis (Hanson 1998, Table 4.1).

6.5 INCUBATION TIME

The incubation time, t_{inc}, is defined as the time at which initiation of a defect due to dry oxidation of the fuel begins. From Section 6.1.6.2, it is clear that the strain necessary for initiation ranges from about 1% (Novak et al. 1983) for a small crack to form, to about 2% (Novak et al. 1983, Nakamura et al. 1995) for gross degradation in CANDU or BWR fuel, to 6.5% (Einziger and Cook 1985) for crack propagation in LWR fuel. For this analysis, it is assumed that zero strain is needed to initiate a defect. Thus, as soon as enough $UO_{2.75}$ (U_3O_8) is formed to touch the cladding, a crack may begin. The incubation time is a function of the fuel/clad gap at the onset of oxidation, the time for the fuel in any local region to oxidize completely to $UO_{2.4}$, t_{24}, and the time for a fraction of the fuel to react to $UO_{2.75}$ until the cladding begins to split. The oxidation times are a function of temperature and the oxidation to $UO_{2.75}$ is also a function of burnup. The time to oxidize to $UO_{2.4}$ is given by (see Section 6.3)

$$t_{2.4}\,(\mathrm{h}) = k_{2.4} \exp(105\ \mathrm{kJ\ mol^{-1}}/RT) \qquad \text{(Eq. 26)}$$

where $k_{2.4}$ is 1.40×10^{-8} (h) for the nominal case or 2.93×10^{-9} (h) for the bounding case (see Table 8) and R is the universal gas constant (8.314 J mol^{-1} K^{-1}) and T is the absolute temperature (K). Sample times at various temperatures were given in Table 9. To convert these times to years, divide $t_{2.4}$ by 8766 (24*365.25).

To calculate the extent of reaction of $UO_{2.4}$ to $UO_{2.75}$ necessary for the fuel to touch the clad, we again start with the volume relation (see Section 6.4.3)

$$r_{21}^3 = z_2\, r_{01}^3 + (1-z_2)\, r_{11}^3 \qquad \text{(Eq. 27)}$$

where z_2 is the volume of $UO_{2.75}$ formed per unit volume of $UO_{2.4}$ reacted (z_2=1.3807, See Table 3). By definition, at t_{inc} the condition $r_{21}=r_C$ exists, where r_C is the inner radius of the cladding.

Since it is assumed that there is no fuel/clad gap at the onset of oxidation, then it holds that $r_C=r_0$. Substituting into Equation 27 gives

$$r_0^3 = z_2\, r_{01}^3 + (1-z_2)\, r_{11}^3 \qquad \text{(Eq. 28)}$$

Since the conversion to $UO_{2.4}$ for any individual grain is complete before oxidation to $UO_{2.75}$ proceeds, it holds that

$$r_{01}^3 = z_1\, r_0^3 \qquad \text{(Eq. 29)}$$

where z_1 is the volume of $UO_{2.4}$ formed per unit volume of UO_2 (z_1=0.9929, see Table 3). Substituting Equation 29 into Equation 28 yields

$$r_{01}^3 /z_1 = z_2\, r_{01}^3 + (1-z_2)\, r_{11}^3 \qquad \text{(Eq. 30)}$$

Solving for r_{11}/r_{01} yields

$$r_{11}/r_{01} = [(1-z_1\, z_2)/(z_1-z_1\, z_2)]^{1/3} \qquad \text{(Eq. 31)}$$

The extent of reaction is thus

$$\lambda_{inc} = 1 - r_{11}/r_{01} = 1-[(1-z_1\, z_2)/(z_1-z_1\, z_2)]^{1/3} = 1-[(V_0-V_8)/(V_9-V_8)]^{1/3} \qquad \text{(Eq. 32)}$$

where V_0, V_9, and V_8 are the volumes of UO_2, $UO_{2.4}$, and $UO_{2.75}$, respectively, as given in Table 3. Substituting these values in Equation 32 gives $\lambda_{inc} = 6.30\times10^{-3}$, which means that only 0.63% of the radius r_{01} reacts to form enough $UO_{2.75}$ for the fuel to touch the clad. Again, this is given the assumptions associated with calculating the volumes (see Section 6.1.2), no fuel/clad gap, no formation of $UO_{2.75}$ until conversion to $UO_{2.4}$ is complete, and zero strain needed for crack initiation.

The time at any fixed temperature for incubation is then

$$t_{inc} = t_{2.4} + \lambda_{inc}\, k_{75} \exp((150+\alpha\times\text{Burnup})\text{kJ}/RT) \qquad \text{(Eq. 33)}$$

where $t_{2.4}$ is given by Equation 26, λ_{inc} is 0.0063, k_{75} is 4.84×10^{-14} (h) for the nominal case or 1.48×10^{-14} (h) for the bounding case (see Table 11), α=1.0 kJ mol^{-1} per MWd/kg M and burnup is in MWd/kg M.

If there is an initial fuel/gap, it can be expressed in terms of a percentage, x, of the original fuel radius. For example, if r_C is 5000 µm and r_0 is 4990 µm (i.e., a 10 µm gap), then x is 10/4990. It is clear then that $r_C=(1+x)r_0$. Similarly, if a strain greater than zero must be present for initiation, it, too, can be expressed as an additional percent s of the original fuel radius that must oxidize. We thus have $r_C=(1+s)r_0$. Since at t_{inc} $r_{21}=r_C$, we can substitute these relations and solve to yield

$$r_{11}/r_{01} = [((1+x)^3\, (1+s)^3 -z_1\, z_2)/(z_1-z_1\, z_2)]^{1/3} \qquad \text{(Eq. 34)}$$

and

$$\lambda_{inc} = 1-[(\{(1+x)^3\ (1+s)^3\ V_0\}-V_8)/(V_9-V_8)]^{1/3} \qquad \text{(Eq. 35)}$$

Note that for the example above (a fuel/clad gap of 10 μm, r_C=5000 μm), λ_{inc} becomes 0.0117. If, in addition, a 1% strain is needed, then λ_{inc} becomes 0.0400 or a factor of 6 longer for incubation time. Finally, if the formation of $UO_{2.4}$ is accompanied by a 2% contraction, as is often reported in literature, then with z_1=0.98 and a fuel/clad gap of zero (x=0) and zero strain (s=0) needed for propagation, then λ_{inc} becomes 0.0182. It is clear that the present assumptions result in conservative incubation times, especially considering the possibility of a higher activation energy for nucleation on the plateau which would significantly increase incubation times. For the zero fuel/clad gap and zero strain case used for this analysis, we can add the times in Table 9 to the times in either Table 12 or Table 13 multiplied by λ_{inc}, 0.0063. Incubation times as a function of temperature and burnup are presented in Table 15 for the nominal case and Table 16 for the bounding case.

Table 15. Incubation Time (yr) as a Function of Temperature and Burnup–Nominal Case

Temperature (°C)	Burnup (MWd/kg M)					
	0	10	20	30	40	50
75	1.04×10^{4}	4.54×10^{4}	1.16×10^{6}	3.63×10^{7}	1.15×10^{9}	3.65×10^{10}
100	8.44×10^{2}	1.70×10^{3}	2.31×10^{4}	5.62×10^{5}	1.41×10^{7}	3.55×10^{8}
125	9.81×10^{1}	1.31×10^{2}	8.10×10^{2}	1.48×10^{4}	3.01×10^{5}	6.18×10^{6}
150	1.49×10^{1}	1.68×10^{1}	4.90×10^{1}	6.03×10^{2}	1.01×10^{4}	1.74×10^{5}
175	2.80×10^{0}	2.95×10^{0}	5.10×10^{0}	3.66×10^{1}	4.99×10^{2}	7.27×10^{3}
195	8.40×10^{-1}	8.63×10^{-1}	1.17×10^{0}	5.13×10^{0}	5.69×10^{1}	7.33×10^{2}
200	6.31×10^{-1}	6.46×10^{-1}	8.37×10^{-1}	3.26×10^{0}	3.41×10^{1}	4.26×10^{2}
225	1.65×10^{-1}	1.67×10^{-1}	1.88×10^{-1}	4.29×10^{-1}	3.12×10^{0}	3.33×10^{1}
250	4.91×10^{-2}	4.94×10^{-2}	5.24×10^{-2}	8.21×10^{-2}	3.79×10^{-1}	3.34×10^{0}
275	1.63×10^{-2}	1.64×10^{-2}	1.69×10^{-2}	2.13×10^{-2}	6.12×10^{-2}	4.20×10^{-1}
283	1.17×10^{-2}	1.17×10^{-2}	1.20×10^{-2}	1.45×10^{-2}	3.64×10^{-2}	2.26×10^{-1}
300	5.96×10^{-3}	5.98×10^{-3}	6.07×10^{-3}	6.86×10^{-3}	1.32×10^{-2}	6.54×10^{-2}
305	4.93×10^{-3}	4.94×10^{-3}	5.01×10^{-3}	5.57×10^{-3}	1.01×10^{-2}	4.63×10^{-2}

Table 16. Incubation Time (yr) as a Function of Temperature and Burnup–Bounding Case

Temperature (°C)	Burnup (MWd/kg M)					
	0	10	20	30	40	50
75	2.28×10^{3}	1.30×10^{4}	3.52×10^{5}	1.11×10^{7}	3.52×10^{8}	1.12×10^{10}
100	1.80×10^{2}	4.41×10^{2}	7.00×10^{3}	1.72×10^{5}	4.32×10^{6}	1.09×10^{8}
125	2.07×10^{1}	3.08×10^{1}	2.38×10^{2}	4.50×10^{3}	9.20×10^{4}	1.89×10^{6}
150	3.13×10^{0}	3.70×10^{0}	1.36×10^{1}	1.83×10^{2}	3.09×10^{3}	5.31×10^{4}
175	5.88×10^{-1}	6.33×10^{-1}	1.29×10^{0}	1.09×10^{1}	1.52×10^{2}	2.22×10^{3}
195	1.76×10^{-1}	1.83×10^{-1}	2.76×10^{-1}	1.49×10^{0}	1.73×10^{1}	2.24×10^{2}
200	1.32×10^{-1}	1.37×10^{-1}	1.95×10^{-1}	9.36×10^{-1}	1.04×10^{1}	1.30×10^{2}
225	3.46×10^{-2}	3.51×10^{-2}	4.17×10^{-2}	1.15×10^{-1}	9.39×10^{-1}	1.02×10^{1}
250	1.03×10^{-2}	1.04×10^{-2}	1.13×10^{-2}	2.04×10^{-2}	1.11×10^{-1}	1.02×10^{0}
275	3.41×10^{-3}	3.43×10^{-3}	3.58×10^{-3}	4.94×10^{-3}	1.72×10^{-2}	1.27×10^{-1}
283	2.45×10^{-3}	2.46×10^{-3}	2.55×10^{-3}	3.32×10^{-3}	9.99×10^{-3}	6.81×10^{-2}
300	1.25×10^{-3}	1.25×10^{-3}	1.28×10^{-3}	1.52×10^{-3}	3.48×10^{-3}	1.94×10^{-2}
305	1.03×10^{-3}	1.03×10^{-3}	1.06×10^{-3}	1.23×10^{-3}	2.61×10^{-3}	1.37×10^{-2}

The model developed for the oxidation transition of $UO_{2.4}$ to $UO_{2.75}$ and the corresponding incubation time was partially validated by comparison of both the model parameters (such as the activation energy derived in Section 6.4.2) and the model output (See Tables 15 and 16) with values obtained from open literature. A comparison of the model predictions for the incubation time with these literature values is made in Table 17. It is clear that some of the experiments performed on the CANDU fuel (Novak et al. 1983; Boase and Vandergraaf 1977) can only be explained by using the bounding case. The presumption is that a hydrated phase may have been present to accelerate the oxidation process. No real comparison with the test by Kohli et al. (1985) can be made because the lack of oxygen during the first 1500 hours of their test would have greatly limited oxidation. The agreement with the data of Nakamura et al. (1995) is within a factor of about 2. The agreement with the whole rod test of Einziger and Cook (1985) is also excellent. For most of the data of EPRI (1986), the agreement of the model predictions with the experimental data ranges from excellent agreement to being too fast (i.e., conservative) by factors in the range 2 to 20. Many of the largest discrepancies can be explained by the very small effective circular diameter of some of the defects, thus greatly inhibiting oxygen transport to the fuel. However, some of the rodlets with the large, drilled hole also had much longer incubation times than the model predicts. These differences can be explained by a combination of a fuel/clad gap, non-zero strain necessary to initiate crack growth, a larger shrinkage of the fuel as it first oxidizes to $UO_{2.4}$, and the unexplained long plateau behavior for some of the samples. Again, agreement with the experimental data is considered quite good given that the model does not need to account for the wide variety of cladding characteristics actually encountered. The assumptions used in this analysis seem reasonable and conservative. Confirmatory data on the behavior of the $UO_{2.4}$ to $UO_{2.75}$ transition provided from additional oxidation tests will further validate the model.

Table 17. Comparison of Incubation Times from Literature with Model

Reference	Temperature (°C)	Burnup (MWd/kg M)	Actual Incubation Time (h)	Model Incubation Time (h)	
				Nominal Case	Bounding Case
Novak	250	0[a]	~600	430	90
Novak	250	0	942<	430	90
Boase	300	0	4<t<7	52	1
Novak	230	7.1	~601	1130	237
Novak	250	7.9	118<t<208	432	90
Kohli[b]	325	17.2	<<2100	21	4
Einziger	229	<11.9	~1000	1200	254
Olsen	217-230	~11.9	<<7206	2240	474
EPRI	295	36	>1676	102	25
EPRI	360	~27	20	7	1
EPRI	360	~27	52<t<60	7	1
EPRI	325	~27	79	22	5
EPRI	325	~27	455	22	5
EPRI	295	~16	55<t<131	64	13
EPRI	295	~21	>80	65	14
EPRI	295	~27	131<t<232	69	15
EPRI	295	~27	386<t<551	69	15
EPRI	283	~8	<140	103	21
EPRI	283	~27	1125	116	25
EPRI	283	~21	~210	106	22
EPRI	283	~27	830	116	25
EPRI	250	~27	~5000	575	134
EPRI	250	~27	9754<t<10545	575	134
EPRI	250	~27	>10545	575	134
Nakamura	200	~14	>11,200	5910	1280
Nakamura	220	~15.7	~4000	1980	425
Nakamura	240	~26.6	~1000	981	234

NOTES: The references correspond to Novak et al. (1983), Boase and Vandergraaf (1977), Kohli et al. (1985), Einziger and Cook (1985), Olsen (1985), EPRI (1986), and Nakamura et al. (1995).

[a] This test was on stainless steel cladding
[b] Limited air greatly reduces the oxidation rate

6.6 UNZIPPING VELOCITY

For times greater than t_{inc}, further oxidation of the $UO_{2.4}$ phase to form $UO_{2.75}$ results in an increasing volume that can further split the cladding. The radial expansion of the fuel is assumed to create the stress necessary to propagate the crack in the axial direction. Since the analysis in Section 6.5 demonstrated that such a small amount of oxidation to $UO_{2.75}$ is needed to initiate a crack, we can assume that further oxidation of the fuel, at least initially, will continue to be isotropic. The extra volume in the axial direction may be accommodated by the relatively large plenum in the fuel rod or by forcing fuel out of the existing crack. While it is more conservative to assume all expansion of the fuel is in the radial direction, such an assumption seems unwarranted at present.

Classical fracture mechanics primarily addresses problems of crack propagation initiation by setting semi-empirical failure criteria. These criteria are usually provided as stress intensity factors; K_I, K_{II}, and K_{III} for the different modes of fracture initiation (Cherepanov 1979, p.59). The K_I, K_{II}, and/or K_{III} stress intensity factors depend on the shape of the body (geometry),

prescribed external loads and/or displacements imposed (boundary conditions), and length of crack(s). The stress intensity factors impose limits to initiate crack propagation on attainable displacements and/or stresses in a local neighborhood of an existing crack or structural flaw. However, for this analysis of cladding unzipping, it is assumed that crack propagation has already been initiated due to oxidation-induced phase-change volume increases near a small flaw/defect that exists through the radial direction of the cladding.

After crack initiation, the crack is assumed to extend or propagate at a quasi-steady rate (means very small speed-acceleration changes) that is slow in comparison to the speed of sound in the cladding material. The rate or speed that the crack propagates axially along the spent fuel rod is evaluated from an analysis of local failure conditions that remain constant if one were to travel in moving reference frame at an arbitrary position of the elastic domain in front of the crack tip (Cherepanov 1979, pp. 200-203). Of these several proposed criteria for local failure; namely, plastic crack tip zone, crack tip radius, crack opening displacement, mean strain over a plastic zone, stress state limit, or "Cherepanov's Generalized Criterion of Local Failure" (Cherepanov 1979, pp. 202-203), all have an equivalence or self-consistency amongst themselves in that a local metric condition at the crack tip must be attained before an existing crack or flaw begins to propagate. Since all of these criteria are self-consistent, a model of crack propagation speed to evaluate the cladding unzipping rate can be formulated from any one of them. To model slow, quasi-steady crack propagation, not only must the local metric condition at the crack tip be attained, but it also must be maintained at a constant value for the crack to continue to propagate at nearly constant speed. For cladding unzipping, the crack opening displacement criterion is the one that leads to a useful and simple result. The resulting crack speed depends on readily accepted material parameters of the elastic shear modulus and the plastic yield stress and on the imposed boundary condition for the opening rate along the crack process zone length. The crack process zone length is shown in Figure 9 and is an axial length along which the phase-change reaction is proceeding to completion. Solid expansion in the zone provides an opening force at the crack tip.

The equation describing the crack propagation velocity is derived as follows: Given the criterion that the crack open relative displacement, u], normal to the symmetry plane of the crack and the displacement at an arbitrary point x(t) moving within the elastic zone ahead of the crack tip is maintained at a constant value during crack propagation, then it follows from differential calculus that the total time derivative of u] is zero if the time derivative of x(t) is equal to the crack velocity. In equation form this is:

$$d(u](x(t),t))/dt = \partial(u](x(t),t))/\partial t + \{\partial(u](x(t),t))/\partial x\}\{\partial x(t)/\partial t\} = 0 \qquad \text{(Eq. 36)}$$

where $\partial x(t)/\partial t$ equals the crack velocity v_2 for the coordinate axis that is shown in Figure 10.

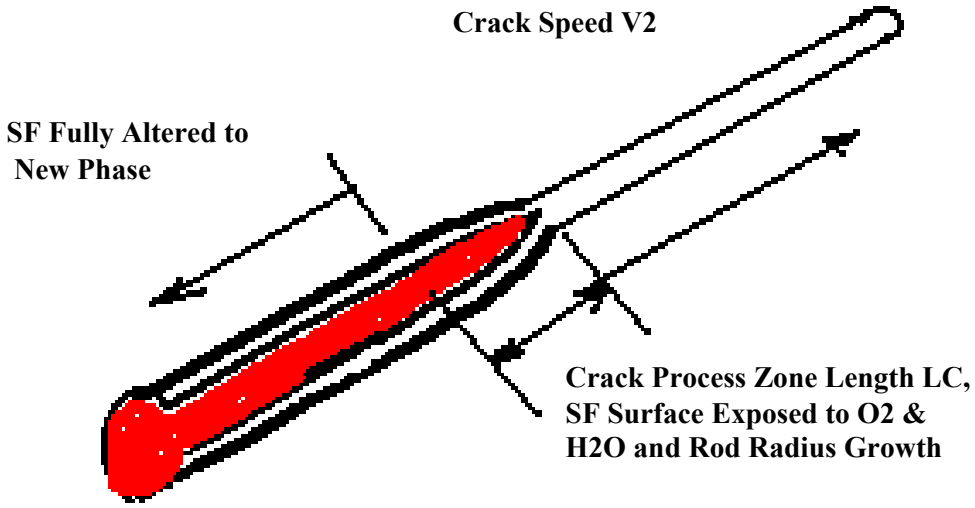

Figure 9. Spent Fuel Rod Showing the Crack Process Zone at Which the Crack Propagation Is Driven by Dry Oxidation and Expansion of the U_3O_8

Thus, for this restricted coordinate system the axial crack velocity component is related to the $u_3]$ crack opening rate and the spatial derivative of the $u_3]$ crack opening with respect to the x_2 coordinate by:

$$v_2 = -\{\partial\,(u_3](x(t),t))/\partial t\}/\{\partial(u_3](x(t),t))/\partial x_2\} \qquad \text{(Eq. 37)}$$

The (32) second order tensor term $\partial\,(u_3](x(t),t))/\partial x_2$, is related to the (32) component of elastic strain in the elastic domain ahead of the crack. (See Sokolnikoff 1956, pp. 20-25.) Because of the localized nature of fracture mechanics, the $u_2]$ relative displacement component ahead of the crack is small, and the (32) component of elastic strain, γ_{32}, is reduced to:

$$\begin{aligned}\gamma_{32} &= \tfrac{1}{2}\{\partial(u_3](x(t),t))/\partial x_2 + \partial(u_2](x(t),t))/\partial x_3\} \\ &= \tfrac{1}{2}\{\partial\,(u_3](x(t),t))/\partial x_2\}\end{aligned} \qquad \text{(Eq. 38)}$$

The (32) component of the stress tensor is related to the (32) component of the strain by the elastic shear modulus G (see Sokolnikoff 1956, p.71):

$$\sigma_{32} = 2G\,\gamma_{32} = G\,\{\partial(u_3](x(t),t))/\partial x_2\} \qquad \text{(Eq. 39)}$$

Since the point x(t) is an arbitrary position in front of the crack, the point x(t) can be taken arbitrarily close to the plastic zone of the crack tip, then the σ_{32} component of shear stress can be evaluated as equal in magnitude to the plastic yield stress σ_{yield}, where the sign of the stress magnitude value is minus. From the above equations, the crack velocity is given in terms of the elastic shear modulus and the yield stress as:

$$v_2 = \{G/\sigma_{32}\}\,\{\partial(u_3](x(t),t))/\partial t\} = \{G/\sigma_{yield}\}\,\{\partial(u_3](x(t),t))/\partial t\} \qquad \text{(Eq. 40)}$$

The final step is relating the rate of opening $\{\partial(u_3](x(t),t))/\partial t\}$ at x(t) to the rate of opening on the boundary of the crack $\{\partial(u_3]/\partial t\}$. For this model of crack propagation velocity, these are assumed to be equal to each other.

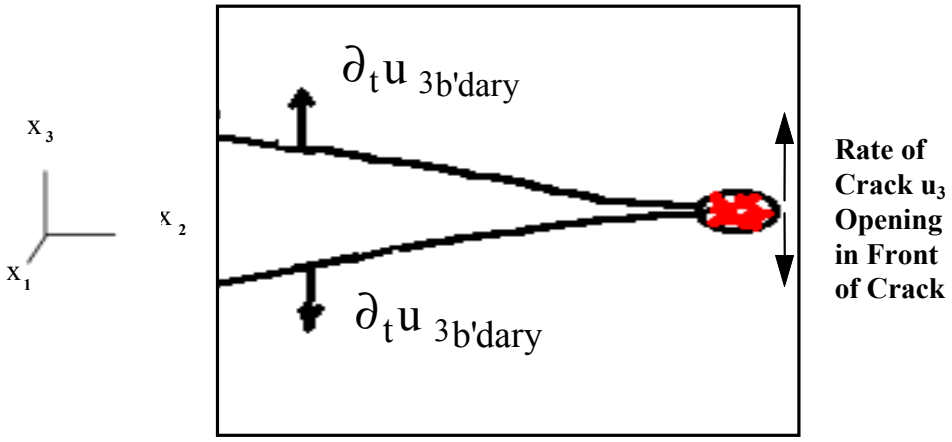

Crack Speed $v_2 = -\partial_t u_3 / \partial_{x_2} u_3$

Note: (u_1, u_2, u_3) is a coordinate system anchored in the cladding. (x_1, x_2, x_3) is a Cartesian space coordinate system. As the interior solid spent fuel is exposed and reacted, its expansion causes the cladding crack to open carrying the solid cladding with it. At the same time, the crack extends in the x_2 direction. A large-scale, almost-steady-state pattern of stress and displacement is moving steadily in the x_2 direction.

Figure 10. A Close-Up of the Crack Process Zone and the Crack Tip

The unzipping velocity of the cladding is thus assumed to be:

$$v = G/\sigma_{yield} \{dr/dt\} \quad \text{(Eq. 41)}$$

where G/σ_{yield} is given by Equations 3 through 6 in Section 6.1.4, and dr/dt is the time-rate-of-change in the radial expansion of the fuel at the crack tip. In this case, the radius of interest is r_{21}, the radius of the $UO_{2.4}$ and $UO_{2.75}$ mixture at time t. Remembering from Section 6.4.3 that:

$$r_{21}^3 = z_2 r_{01}^3 + (1-z_2) r_{11}^3 \quad \text{(Eq. 20)}$$

$$r_{11}/r_{01} = [\ 1 + (((\rho_{2.0}/z_1)\ \Delta(O/M)\ (16/270))/(\rho_{2.4} - z_2\ \rho_{2.75}\ ))]^{1/3} \quad \text{(Eq. 22)}$$

$$\lambda_{75} = 1 - r_{11}/r_{01} \quad \text{(Eq. 23)}$$

$$t_{\Delta(O/M)75} = \lambda_{75}\ k_{75}\ \exp(Q_{75}/RT) \quad \text{(Eq. 25)}$$

we can use the forward difference method to approximate dr/dt as $\Delta r/\Delta t$. This approximation is valid for small changes in Δ(O/M), with corresponding small changes in Δr and Δt, and for times shortly after t_{inc}. Choosing two close values of Δ(O/M) results in the equation:

$$\Delta r/\Delta t = \{(r_{21b}/r_{01} - r_{21a}/r_{01})\, r_{01}\}/\{(\lambda_b - \lambda_a)\, k_{75} \exp(Q_{75}/RT)\} \quad \text{(Eq. 42)}$$

We can solve for r_{21}/r_{01} using Equations 22 and 20 to obtain:

$$r_{21}/r_{01} = [1 + (((\rho_{2.0}/z_1)\, \Delta(O/M)\, (16/270)\, (1-z_2))/(\rho_{2.4} - z_2\, \rho_{2.75}))]^{1/3} \quad \text{(Eq. 43)}$$

Solving Equation 22 for Δ(O/M) given an extent of conversion λ_{inc}=0.0063, yields a value of 0.0066 or a bulk O/M of about 2.407. For the forward difference method we shall use the values of Δ(O/M) of 0.01 (bulk O/M=2.41) and 0.02 (bulk O/M=2.42). By inserting the values of Δ(O/M) into Equations 43 and 22 and then using Equation 23 to solve for λ, we have all the information necessary to solve Equation 42. Note that Equation 42 is the first equation where a real dimension (either r_{21} or r_{01}) is needed as opposed to the dimensionless ratios of the radii in the other equations. However, this model is semi-empirical, not mechanistic, and a "non-realistic" dimension can be chosen for the grain radius and still be valid. For simplicity, the single grain approximation to the fuel pellet was assumed. This eliminates the need to determine the number of grains that are impacting the radial expansion. Thus, the value of 0.5 cm, representative of an average inner cladding radius (see Table 4) was chosen for the initial radius r_{01} of the $UO_{2.4}$ grain. Unzipping velocities at a variety of temperatures and burnups are reported in Table 18 where it was assumed that there are 8766 hours per year. A typical fuel rod has a nominal active fuel length (See Table 4) of about 350 cm. Assuming a defect at the midpoint of the active fuel length, the total time to fully unzip a rod at 200°C varies from a little over 1 year at 0 burnup to 3.8×10^5 years at a burnup of 50 MWd/kg M. At 100°C, the times to unzip for similar burnups are 4.1×10^4 years and 4.1×10^{11} years, respectively.

Table 18. Unzipping Velocity (cm yr^{-1}) as a Function of Temperature and Burnup- Nominal Case

Temperature (°C)	Burnup (MWd/kg M)					
	0	10	20	30	40	50
75	1.26×10^{-4}	3.97×10^{-6}	1.25×10^{-7}	3.95×10^{-9}	1.25×10^{-10}	3.93×10^{-12}
100	4.29×10^{-3}	1.70×10^{-4}	6.78×10^{-6}	2.70×10^{-7}	1.07×10^{-8}	4.26×10^{-10}
125	9.46×10^{-2}	4.61×10^{-3}	2.24×10^{-4}	1.09×10^{-5}	5.32×10^{-7}	2.59×10^{-8}
150	1.46×10^{0}	8.52×10^{-2}	4.96×10^{-3}	2.89×10^{-4}	1.68×10^{-5}	9.79×10^{-7}
175	1.68×10^{1}	1.15×10^{1}	7.83×10^{-2}	5.35×10^{-3}	3.65×10^{-4}	2.49×10^{-5}
200	1.51×10^{2}	1.19×10^{1}	9.34×10^{-1}	7.34×10^{-2}	5.77×10^{-3}	4.54×10^{-4}
225	1.10×10^{3}	9.82×10^{1}	8.78×10^{0}	7.84×10^{-1}	7.00×10^{-2}	6.26×10^{-3}
250	6.70×10^{3}	6.72×10^{2}	6.74×10^{1}	6.76×10^{0}	6.78×10^{-1}	6.79×10^{-2}
275	3.51×10^{4}	3.91×10^{3}	4.35×10^{2}	4.85×10^{1}	5.40×10^{0}	6.01×10^{-1}
300	1.62×10^{5}	1.98×10^{4}	2.43×10^{3}	2.98×10^{2}	3.65×10^{1}	4.47×10^{0}
350	2.52×10^{6}	3.65×10^{5}	5.30×10^{4}	7.68×10^{3}	1.11×10^{3}	1.62×10^{2}

The model predictions for the unzipping velocity were partially validated by comparison in Table 19 with the unzipping velocities reported in literature (see Table 6). Other than the CANDU fuel of zero burnup (Boase and Vandergraaf 1977) and the BWR rod tested by Kohli et al. (1985), which would have oxidized much faster had ample oxygen been present, the model

predictions agree with the experimental data within a factor of 28. Most of the data points agree within a factor of 10 and only two of the predictions are not conservative, which is to be expected since the nominal case parameters were for a best fit to data and not conservative for all cases. If irradiated properties of Zircaloy are used, the model unzipping velocities would decrease by a factor of 2 to 3 (see Section 6.1.4). The model with its conservative assumptions appears to predict unzipping velocities that are both reasonable and, for the most part, conservative. However, the lowest temperature tested was 230°C, so the results at the temperatures of interest to the repository are extrapolations that have not been verified. The activation energies chosen for the oxidation reactions, though, are conservative at the lower temperatures as long as there is not a change in mechanism or activation energy below the temperatures tested. Confirmatory data from additional oxidation tests will further validate the model by providing additional information of the oxidation kinetics over a broader range of temperatures.

Table 19. Comparison of Unzipping Velocities from Literature with Model

Reference	Temperature (°C)	Burnup (MWd/kg M)	Actual Unzipping Velocity (cm min^{-1})	Unzipping Velocity (cm min^{-1})-Nominal Case	Model/ Experimental
Boase	300	0	1.2×10^{-4}	3.1×10^{-1}	2583
Novak	230	7.9	2.3×10^{-5}	4.6×10^{-4}	20
Novak	250	7.9	1.2×10^{-4}	2.1×10^{-3}	18
Boase	250	7.8-8.6	$\sim1\times10^{-4}$	1.9×10^{-3}	19
Kohli[a]	325	17.2	$<1.9\times10^{-4}$	4.0×10^{-2}	210
Einziger	229	<11.9	$<3\times10^{-5}$	1.6×10^{-4}	5
EPRI	360	~27	2.3×10^{-3}	4.7×10^{-2}	20
EPRI	360	~27	$>1.7\times10^{-3}$	4.7×10^{-2}	28
EPRI	325	~27	1.4×10^{-3}	5.6×10^{-3}	4
EPRI	325	~27	1.4×10^{-3}	5.6×10^{-3}	4
EPRI	295	~16	$>1.2\times10^{-3}$	7.7×10^{-3}	6
EPRI	295	~21	1.0×10^{-3}	2.7×10^{-3}	3
EPRI	295	~27	$>9.8\times10^{-4}$	7.5×10^{-4}	0.8
EPRI	295	~27	$>4.4\times10^{-4}$	7.5×10^{-4}	2
EPRI	283	~8	1.0×10^{-3}	1.9×10^{-2}	19
EPRI	283	~27	4.8×10^{-4}	3.2×10^{-4}	0.7
EPRI	283	~21	4.0×10^{-4}	1.2×10^{-3}	3
EPRI	283	~27	3.0×10^{-4}	3.2×10^{-4}	1

NOTES: The references correspond to Novak et al. (1983), Boase and Vandergraaf (1977), Kohli et al. (1985), Einziger and Cook (1985), and EPRI (1986).

[a] Limited air greatly reduces the oxidation rate

TableCurve was used to fit the logarithm of the actual unzipping velocities (except for the zero burnup data point) as a function of inverse temperature (DTN: LL000402951021.133). An activation energy of –81.3 kJ mol^{-1} (R^2=0.75) was obtained, which corresponds nicely with the value of –77.0 kJ mol^{-1} reported by Einziger (1994, Equation 3) for a fit of mostly the same data. The model predictions were then fitted, again neglecting the zero burnup data point, and an activation energy of –92.0 kJ mol^{-1} (R^2=0.55) was obtained. Note that the model predictions have multiple data points that are identical at some of the temperatures because the burnups are the same, thus there is a heavier weighting to those points. It is important to note that this activation energy is not equal to the activation energy of the oxidation from $UO_{2.4}$ to $UO_{2.75}$ because the cladding properties are also a function of temperature, and these terms are thus

included in the 1/T fit. It is also important to stress that these values represent an activation energy for unzipping velocities for the range of burnup and temperatures reported. Low-burnup fuels would reduce the activation energy for the oxidation of the fuel and, correspondingly, reduce the activation energy for unzipping velocity. High-burnup fuels, on the other hand, would increase this activation energy. Similar biases would result by including much lower or much higher temperatures where the cladding properties could change significantly, thus affecting the calculated overall activation energy. Still, the model predictions obtained by fits of TGA data agree fairly well and conservatively with the actual incubation and unzipping data from literature.

6.6.1 Alternative Approach for Unzipping Velocity Calculation

Starting with Equation 43, the values of r_{21} for two different values of $\Delta(O/M)$ were calculated using a forward difference method. The change in the radius can then be expressed as:

$$\Delta r_{21} = r_{01}\,[1+1.0882\,\Delta(O/M)_b]^{1/3} - r_{01}\,[1+1.0882\,\Delta(O/M)_a]^{1/3} \qquad \text{(Eq. 44)}$$

where the appropriate values of densities and z_1 and z_2 (from Table 3) have been substituted. Using a Taylor series expansion for the right hand side of the equation yields:

$$\Delta r_{21} = r_{01}[1+1/3\bullet 1.0882\,\Delta(O/M)_b - 2/18\bullet(1.0882\,\Delta(O/M)_b)^2+10/16\bullet(1.0882\,\Delta(O/M)_b)^3] - r_{01}[1+1/3\bullet 1.0882\,\Delta(O/M)_a - 2/18\bullet(1.0882\,\Delta(O/M)_a)^2+10/16\bullet(1.0882\,\Delta(O/M)_a)^3] \qquad \text{(Eq. 45)}$$

At very early times after t_{inc}, the approximation using only the first order term is valid with only a few percent error. The approximation is:

$$\Delta r_{21} = r_{01}[0.3627\,(\Delta(O/M)_b - \Delta(O/M)_a)] \qquad \text{(Eq. 46)}$$

Similarly,

$$\Delta t = (\lambda_b - \lambda_a) k_{75} \exp(Q_{75}/RT) \qquad \text{(Eq. 47)}$$

where

$$\lambda = 1 - r_{11}/r_{01} \qquad \text{(Eq. 48)}$$

A similar Taylor series expansion and truncation yields:

$$\lambda_b - \lambda_a = 1 - [1 - 1/3\bullet 2.8584\,\Delta(O/M)_b] - \{1 - [1 - 1/3\bullet 2.8584\,\Delta(O/M)_a]\} \qquad \text{(Eq. 49)}$$

Again, only for very early times after t_{inc}:

$$\Delta r_{21}/\Delta t = r_{01}\,[0.3627\,(\Delta(O/M)_b - \Delta(O/M)_a)]/ \{[0.9528\,(\Delta(O/M)_b - \Delta(O/M)_a)]\,k_{75}\exp(Q_{75}/RT)\} \qquad \text{(Eq. 50)}$$

If a value of 0.5 cm for r_{01} is chosen, then at very early times after t_{inc}:

$$\Delta r_{21}/\Delta t = 0.1903 \times Rate_{75} \qquad \text{(Eq. 51)}$$

where $$Rate_{75} = 1/\{k_{75} \exp(Q_{75}/RT)\}$$ (Eq. 52)

Since the unzipping velocity is found by multiplying (G/σ_{yield}) by $(\Delta r_{21}/\Delta t)$, the following unzipping velocities, given in Table 20, are calculated for a specified temperature, remembering that the rate is both burnup and temperature dependent.

Table 20. Alternative Unzipping Velocities (cm hr^{-1})

Temperature (°C)	G/σ_{yield}	Unzipping Velocity (cm hr^{-1})
100	131	25 $Rate_{75}$
150	147	28 $Rate_{75}$
200	168	32 $Rate_{75}$
250	194	37 $Rate_{75}$
300	231	44 $Rate_{75}$

Again, if the properties of irradiated Zircaloy are used, the unzipping velocities will be reduced by a factor of 2 to 3.

7. CONCLUSIONS

A semi-empirical model has been developed to calculate the time to oxidize a sample from UO_2 to $UO_{2.4}$, the time to oxidize from $UO_{2.4}$ to $UO_{2.75}$, and the subsequent incubation times for oxidation of spent fuel to initiate crack growth at an existing defect and then the velocity at which that crack will propagate. The model was developed by fitting the data obtained by TGA testing of spent fuel fragments over the temperature range 255°C to 325°C in a dry-air atmosphere. The fuels tested and used in this analysis had burnups in the range 16 MWd/kg M to about 42 MWd/kg M. It is assumed that extrapolations outside of both the temperature and burnup ranges are valid, i.e., that there is no change in activation energy or mechanism in either case.

The model developed both nominal and bounding case fits to the data. The nominal fit can be used for moderate to high burnup fuels that are known to be free of hydrated phases. The bounding case fit can be used for low burnup fuels and for those known to have hydrated phases present. It is assumed that the presence of moisture during oxidation will increase the oxidation rate, but that this rate is within the bounding case presented. Confirmatory testing is underway to validate this assumption. Oxidation of the fuel proceeds from UO_2 to $UO_{2.4}$ until a grain is fully converted, at which point formation of $UO_{2.75}$ begins. Based on analysis of TGA data, the appropriate equations and parameters to use for clad degradation due to fuel oxidation follow:

$\underline{UO_2 \rightarrow UO_{2.4}}$

$$t_{2.4} = k_{2.4} \exp(Q_{24}/RT)$$

where

$t_{2.4}$ is the time to oxidize from UO_2 to $UO_{2.4}$ (h)

$k_{2.4}$ is the pre-exponential factor for the UO_2 to $UO_{2.4}$ transition (h)

Nominal Case: 1.40×10^{-8}

Bounding Case: 2.93×10^{-9}

Q_{24} is the corresponding activation energy (105 kJ mol^{-1})

R is the universal gas constant (8.314 J mol^{-1} K^{-1})

and T is the temperature (K =273+T(°C)).

$\underline{UO_{2.4}\rightarrow UO_{2.75}}$

$$t_{2.75} = k_{75} \exp(\{Q_{75}^{0}+\alpha\times\text{Burnup}\}/RT)$$

where

$t_{2.75}$ is the time to oxidize from $UO_{2.4}$ to $UO_{2.75}$ (h)

k_{75} is the pre-exponential factor for the $UO_{2.4}$ to $UO_{2.75}$ transition (h)

Nominal Case: 4.84×10^{-14}

Bounding Case: 1.48×10^{-14}

Q_{75}^{0} is the corresponding Arrhenius activation energy (150 kJ mol^{-1})

α=1.0 kJ mol^{-1} per MWd/kg M

Burnup is the local burnup of the sample (MWd/kg M)

R is the universal gas constant (8.314 J mol^{-1} K^{-1})

and T is the temperature (K =273+T(°C)).

The incubation time, or time for the oxidation of fuel to start stressing the cladding such that crack initiation at the defect begins can be calculated by

$$t_{inc} = t_{2.4} + \lambda_{inc}\, k_{75} \exp((150+\alpha\times\text{Burnup})\text{kJ}/RT)$$

where

t_{inc} is the incubation time (h)

and λ_{inc} is the extent of reaction of $UO_{2.4}$ to $UO_{2.75}$ for the fuel to stress the cladding. In the present analysis, for a zero fuel/clad gap and zero strain to initiate a crack, λ_{inc}=0.0063. In other cases, λ_{inc} may be calculated as

$$\lambda_{inc} = 1-[(\{(1+x)^3\,(1+s)^3\,V_0\}-V_8)/(V_9-V_8)]^{1/3}$$

where x is the percent of the original fuel radius to represent the fuel/clad gap, s is the percent strain necessary to initiate a crack, and V_0, V_9, and V_8 are the volumes of the UO_2, $UO_{2.4}$, and $UO_{2.75}$ phases on a per mol U basis.

Finally, the unzipping velocity of the crack due to fuel oxidation can be expressed as

$$v = G/\sigma_{yield}\ \{dr/dt\}$$

where v is the unzipping velocity (cm hr^{-1}), G/σ_{yield} is the elastic shear modulus divided by the yield strength of the Zircaloy, and dr/dt is the time-rate-of-change in the radial expansion of the fuel at the crack tip. In this case, the radius of interest is r_{21}, the radius of the $UO_{2.4}$ and $UO_{2.75}$

mixture at time t. Since dr/dt can be approximated as $\Delta r/\Delta t$, we can solve for the unzipping velocity using

$$\Delta r/\Delta t = \{(r_{21b}/r_{01} - r_{21a}/r_{01})\, r_{01}\}/\{(\lambda_b - \lambda_a)\, k_{75} \exp((Q_{75}^{0} + \alpha \times \text{Burnup})/RT)\}$$

$$\lambda_{a,b} = 1 - r_{11a,b}/r_{01}$$

$$r_{11a,b}/r_{01} = [\,1 + ((\rho_{2.0}/z_1\, \Delta(O/M)_{a,b}\, (16/270))/(\rho_{2.4} - z_2\, \rho_{2.75}))]^{1/3}$$

$$r_{21a,b}/r_{01} = [\,1 + ((\rho_{2.0}/z_1\, \Delta(O/M)_{a,b}\, (16/270)\, (1-z_2))/(\rho_{2.4} - z_2\, \rho_{2.75}))]^{1/3}$$

where $\rho_{2.0}$, $\rho_{2.4}$, and $\rho_{2.75}$ are the densities of the UO_2, $UO_{2.4}$, and $UO_{2.75}$ phases, respectively, and z_1 and z_2 are equal to V_9/V_0 and V_8/V_9, respectively.

The incubation times and unzipping velocities are very strongly temperature and burnup dependent. The incubation times and unzipping velocities were developed using only qualified data. These values predicted by the model were partially validated by comparison with values reported in open literature. For the most part, the model predictions were reasonable and conservative. Confirmatory data obtained from additional oxidation tests will further validate the model.

This document may be affected by technical product input information that requires confirmation. Any changes to the document that may occur as a result of completing the confirmation activities will be reflected in subsequent revisions. The status of the input information quality may be confirmed by review of the Document Input Reference System database.

8. INPUTS AND REFERENCES

8.1 DOCUMENTS CITED

Boase, D.G. and Vandergraaf, T.T. 1977. "The Canadian Spent Fuel Storage Canister: Some Materials Aspects." *Nuclear Technology, 32,* 60-71. La Grange Park, Illinois: American Nuclear Society. TIC: 237173.

Cherepanov, G.P. 1979. *Mechanics of Brittle Fracture.* 200-203. New York, New York: McGraw-Hill. On Order Library Tracking Number-L1417

Choi, J.W.; McEachern, R.J.; Taylor, P.; and Wood, D.D. 1996. "The Effects of Fission Products on the Rate of U3O8 Formation in SIMFUEL Oxidized in Air at 250°C." *Journal of Nuclear Materials, 230,* 250-258. Amsterdam, The Netherlands: Elsevier Science. TIC: 246437.

CRWMS M&O 1998. *Design Basis Cladding Analysis.* BBA000000-01717-0200-00054 REV 01. Las Vegas, Nevada: CRWMS M&O. ACC: MOL.19980325.0102.

CRWMS M&O 1999a. *Classification of the MGR Uncanistered Spent Nuclear Fuel Disposal Container System.* ANL-UDC-SE-000001 REV 00. Las Vegas, Nevada: CRWMS M&O. ACC: MOL.19990928.0216.

CRWMS M&O 1999b. *1101213FM3 Waste Form Analyses & Models - PMR.* Activity Evaluation, December 14, 1999. Las Vegas, Nevada: CRWMS M&O. ACC: MOL.19991217.0048.

CRWMS M&O 2000. *Waste Package Materials Department Analysis and Modeling Reports Supporting the Waste Form PMR*. Development Plan TDP-EBS-MD-000005 REV 01. Las Vegas, Nevada: CRWMS M&O. ACC: MOL.20000202.0173.

Davis, R.B. and Pasupathi, V. 1981. *Data Summary Report for the Destructive Examination of Rods G7, G9, J8, I9, and H6 from Turkey Point Fuel Assembly B17.* HEDL-TME 80-85. Richland, Washington: Westinghouse Hanford Co. TIC: 216800.

Dieter, G.E. 1961. *Mechanical Metallurgy.* 1st Edition. New York, New York: McGraw-Hill Book Company. TIC: 245037.

DOE (U.S. Department of Energy) 2000. *Quality Assurance Requirements and Description.* DOE/RW-0333P, Rev. 9. Washington, D.C.: U.S. Department of Energy, Office of Civilian Radioactive Waste Management. ACC: MOL.19991028.0012.

Einziger, R.E. 1994. "Preliminary Spent LWR Fuel Oxidation Source Term Model." *High Level Radioactive Waste Management, Proceedings of the Fifth Annual International Conference, Las Vegas, Nevada, May 22-26, 1994. 2,* 554-559. La Grange Park, Illinois: American Nuclear Society. TIC: 210984.

Einziger, R.E. and Cook, J.A. 1985. "Behavior of Breached Light Water Reactor Spent Fuel Rods in Air and Inert Atmospheres at +229 degrees Celsius." *Nuclear Technology, 69,* 55-71. La Grange Park, Illinois: American Nuclear Society. TIC: 242380.

Einziger, R.E.; Marschman, S.C.; and Buchanan, H.C. 1991. "Spent-Fuel Dry-Bath Oxidation Testing." *Nuclear Technology, 94,* 383-393. Hinsdale, Illinois: American Nuclear Society. TIC: 246459.

Einziger, R.E.; Thomas, L.E.; Buchanan, H.C.; and Stout, R.B. 1992. "Oxidation of Spent Fuel in Air at 175 to 195°C." *Journal of Nuclear Materials, 190,* 53-60. Amsterdam, The Netherlands: North-Holland Publishing Company. TIC: 238511.

EPRI (Electric Power Research Institute) 1986. *Oxidation of Spent Fuel Between 250 and 360°C.* EPRI NP-4524. Palo Alto, California: Electric Power Research Institute. TIC: 228313.

Glasstone, S. and Sesonske, A. 1994. *Nuclear Reactor Engineering, Reactor Design Basics.* 4th Edition. Volume One. pp. 449-451, 461. Amsterdam, The Netherlands: Kluwer Academic Publishers. TIC: 246137.

Gray, W.J. and Wilson, C.N. 1995. *Spent Fuel Dissolution Studies FY 1991-1994.* PNL-10450. Richland, Washington: Pacific Northwest Laboratory. ACC: MOL.19960802.0035.

Guenther, R.J.; Blahnik, D.E.; Campbell, T.K.; Jenquin, U.P.; and Mendel, J. 1988a. *Characterization of Spent Fuel Approved Testing Material–ATM-103.* PNL-5109-103. Richland, Washington: Pacific Northwest Laboratory. TIC: 223979.

Guenther, R.J.; Blahnik, D.E.; Campbell, T.K.; Jenquin, U.P.; Mendel, J.E.; and Thornhill, C.K. 1988b. *Characterization of Spent Fuel Approved Testing Material –ATM-106.* PNL-5109-106. Richland, Washington: Pacific Northwest Laboratory. TIC: 223978.

Guenther, R.J.; Blahnik, D.E.; Jenquin, U.P.; Mendel, J.E.; Thomas, L.E.; and Thornhill, C.K. 1991a. *Characterization of Spent Fuel Approved Testing Material –ATM-104.* PNL-5109-104. Richland, Washington: Pacific Northwest Laboratory. TIC: 203846.

Guenther, R.J.; Blahnik, T.K.; Campbell, T.K.; Jenquin, U.P.; and Mendel, J.E. 1991b. *Characterization of Spent Fuel Approved Testing Material-ATM-105.* PNL-5109-105. Richland, Washington: Pacific Northwest Laboratory. TIC: 203785.

Hanson, B.D. 1998. *The Burnup Dependence of Light Water Reactor Spent Fuel Oxidation.* PNNL-11929. Richland, Washington: Pacific Northwest National Laboratory. TIC: 238459.

Johnson, L.H. and Taylor, P. 1998. *Alteration of Spent CANDU Fuel in Aerated Steam at 150°C.* Draft. Pinawa, Manitoba, Canada: Atomic Energy of Canada Limited. ACC: MOL.19981118.0337.

Kansa, E.J.; Hanson, B.D.; and Stout, R.B. 1998. *Grain Size and Burnup Dependence of Spent Fuel Oxidation: Geological Repository Impact*. UCRL-JC-131592. Livermore, California: Lawrence Livermore National Laboratory. ACC: MOL.19990420.0128.

Kohli, R.; Stahl, D.; Pasupathi, V.; Johnson, A.B.; and Gilbert, E.R. 1985. "The Behavior of Breached Boiling Water Reactor Fuel Rods on Long-Term Exposure to Air and Argon at 598 K." *Nuclear Technology, 69,* 186-197. La Grange Park, Illinois: American Nuclear Society. TIC: 245332.

McEachern, R.J. and Taylor, P. 1998. "A Review of the Oxidation of Uranium Dioxide at Temperatures Below 400°C." *Journal of Nuclear Material, 254,* 87-121. Amsterdam, The Netherlands: Elsevier Science. TIC: 246427.

McEachern, R.J.; Choi, M.; Kolar, M.; Long, W.; Taylor, P.; and Wood, D.D. 1997. "Determination of the Activation Energy for the Formation of U3O8 on UO2." *Journal of Nuclear Materials.* 249. 58-69. Amsterdam , The Netherlands: Elsevier Science.

McEachern, R.J.; Doern, D.C.; and Wood, D.D. 1998. "The Effect of Rare-Earth Fission Products on the Rate of U3O8 Formation on UO2." *Journal of Nuclear Materials, 252,* 145-149. Amsterdam, The Netherlands: Elsevier Science. TIC: 246428.

Mendelson, M.I. 1969. "Average Grain Size in Polycrystalline Ceramics." *Journal of the American Ceramics Society, 52,* (8), 443-446. Westerville, Ohio: American Ceramics Society. TIC: 246642.

Nakamura, J.; Otomo, T.; Kikuchi, T.; and Kawasaki, S. 1995. "Oxidation of Fuel Rod Under Dry Storage Condition." *Journal of Nuclear Science and Technology, 32,* (4), 321-332. Tokyo, Japan: Atomic Energy Society of Japan. TIC: 246641.

Novak, J.; Hastings, I.J.; Mizzan, E.; and Chenier, R.J. 1983. "Postirradiation Behavior of UO2 Fuel I: Elements at 220 to 250 Degrees C in Air." *Nuclear Technology, 63,* 254-263. La Grange Park, Illinois: American Nuclear Society. TIC: 217080.

Olander, D.R.; Kim, Y.S.; Wang, W-E.; and Yagnik, S.K. 1999. "Steam Oxidation of Fuel in Defective LWR Rods." *Journal of Nuclear Materials, (270), 11-20*. New York, New York: Elsevier Science. TIC: 246527.

Olsen, C.S. 1985. *Investigation of the Stability of LWR Spent Fuel Rods Below 250°C.* NUREG/CR-4345. Washington , D.C.: U.S. Nuclear Regulatory Commission. TIC: 246556.

Sokolnikoff, I.S. 1956. *Mathematical Theory of Elasticity.* 2nd edition. New York, New York: McGraw-Hill. TIC: 240386.

Stout, R.B. and Leider, H.R. 1998. *Waste Form Characteristics Report, Revision 1.* UCRL-ID-108314, Version 1.3. Livermore, California: Lawrence Livermore National Laboratory. ACC: MOL.19981214.0043.

Sunder, S. and Miller, N.H. 1996. "Oxidation of CANDU Uranium Oxide Fuel by Air in Gamma Radiation at 150 degrees C." *Journal of Nuclear Materials, 231,* 121-131. Amsterdam, The Netherlands: Elsevier Science. TIC: 246429.

Taylor, P.; Lemire, R.J.; and Wood, D.D. 1993. "The Influence of Moisture on Air Oxidation of UO2: Calculations and Observations." *Nuclear Technology, 104,* 164-170. Hinsdale, Illinois: American Nuclear Society. TIC: 246460.

Taylor, P.; Wood, D.D.; Duclos, A.M.; and Owen, D.G. 1989. "Formation of Uranium Trioxide Hydrates on UO2 Fuel in Air-Steam Mixtures Near 200°C." *Journal of Nuclear Materials, 168,* (1&2), 70-75. Amsterdam, The Netherlands: Elsevier Science. TIC: 246601.

Thomas, L.E. and Einziger, R.E. 1992. "Grain Boundary Oxidation of Pressurized-Water Reactor Spent Fuel in Air." *Materials Characterization, 28,* (2), 149-156. New York, New York: Elsevier Science Publishing Company. TIC: 243294.

Thomas, L.E.; Einziger, R.E.; and Buchanan, H.C. 1993. "Effects of Fission Products on Air Oxidation of LWR Spent Fuel." *Journal of Nuclear Materials, 201,* 310-319. Amsterdam, The Netherlands: Elsevier Science Publishers. TIC: 242662.

Wasywich, K.; Hocking, W.H.; Shoesmith, D.W.; and Taylor, P. 1993. "Differences in Oxidation Behavior of Used CANDU Fuel During Prolonged Storage in Moisture-Saturated Air and Dry Air at 150°C." *Nuclear Technology, 104,* (3), 309-329. La Grange Park, Illinois: American Nuclear Society. TIC: 246598.

Woodley, R.E.; Einzeger, R.E.; and Buchanan, H.C. 1989. "Measurement of the Oxidation of Spent Fuel Between 140 and 225 Degrees C." *Nuclear Technology, 85,* (1), 74-88. La Grange Park, Illinois: American Nuclear Society. TIC: 243577.

8.2 CODES, STANDARDS, REGULATIONS, AND PROCEDURES

ASTM C 1174-97. 1997. *Standard Practice for Prediction of the Long-Term Behavior of Materials, Including Waste Forms, Used in Engineered Barrier Systems (EBS) for Geological Disposal of High-Level Radioactive Waste.* West Conshohocken, Pennsylvania: American Society for Testing and Materials. TIC: 246015.

AP-3.10Q, Rev. 02, ICN 0. *Analyses and Models.* Washington D.C., Washington D.C.: Office of Civilian Radioactive Waste Management. ACC: MOL.20000217.0246.

QAP-2-3, Rev. 10. *Classification of Permanent Items.* Las Vegas, Nevada: CRWMS M&O. ACC: MOL.19990316.0006.

QAP-2-0, Rev. 5, ICN 1. *Conduct of Activities.* Las Vegas, Nevada: CRWMS M&O. ACC: MOL.19991109.0221.

8.3 SOURCE DATA

LL000314651021.132. Cladding Degradation-Dry Unzipping. Submittal date: 03/25/2000.

LL000402951021.133. Data from Laboratory Record Book. Regression Analysis of Dry Oxidation. Submittal date: 04/13/2000.